In-medium effect on the *NN* inelastic cross sections in HICs at intermediate energies

Pengcheng Li

Huzhou Normal University

Based on: P. C. Li, A. B. Larionov, Y. J. Wang, G. C. Yong, Q. F. Li, arXiv:2609.25818 [nucl-th]



Contents

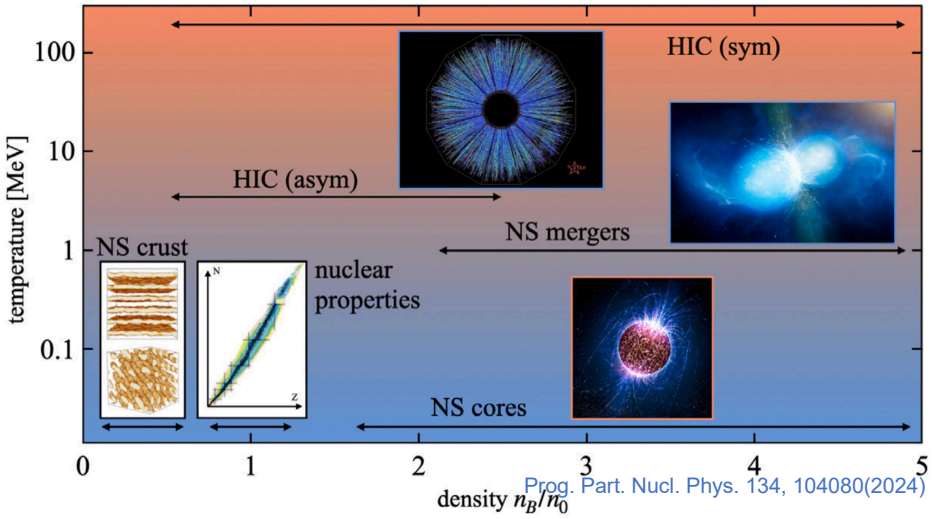
01 Introduction

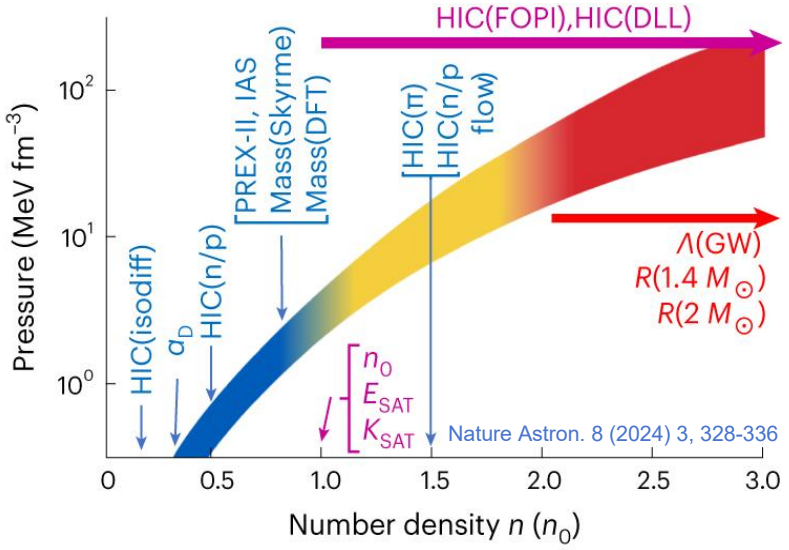
02 Methodology

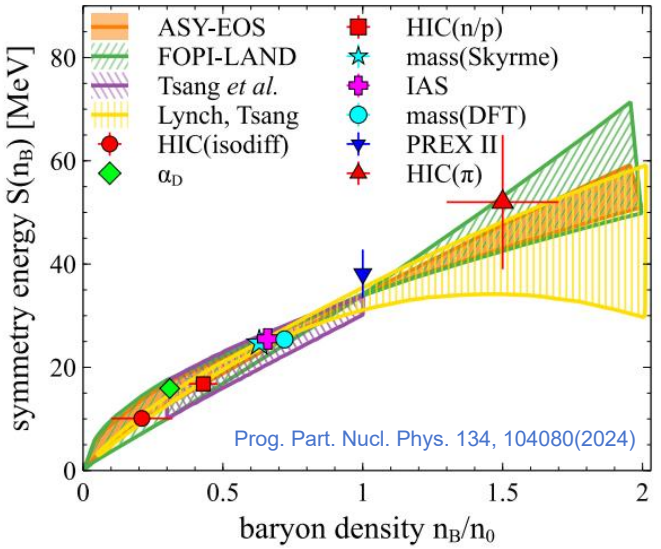
03 Results and discussion

04 Summary and outlook

1.1 Background







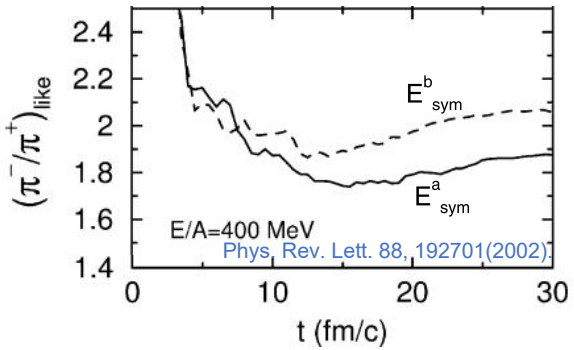
- The equation of state (EoS) is a fundamental property of nuclear matter, controls the structure of nuclei, determines the properties of nuclear matter at extreme conditions (produced in HICs, observed in neutron stars).
- However, tight constraints on both the symmetric and asymmetric EoS at higher densities have so far remained elusive.

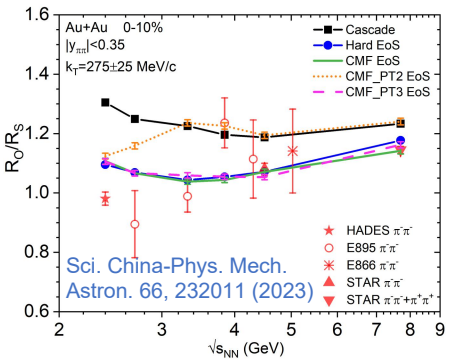
INSTITUTE OF PHYSICS PUBLISHING JOURNAL OF PHYSICS G: NUCLEAR AND PARTICLE PHYSICS

J. Phys. G: Nucl. Part. Phys. **32** (2006) 151–164 doi:10.1088/0954-3899/32/2/007

Probing the equation of state with pions

Qingfeng Li[1], Zhuxia Li[2], Sven Soff[3], Marcus Bleicher[3] and Horst Stöcker[1,3]



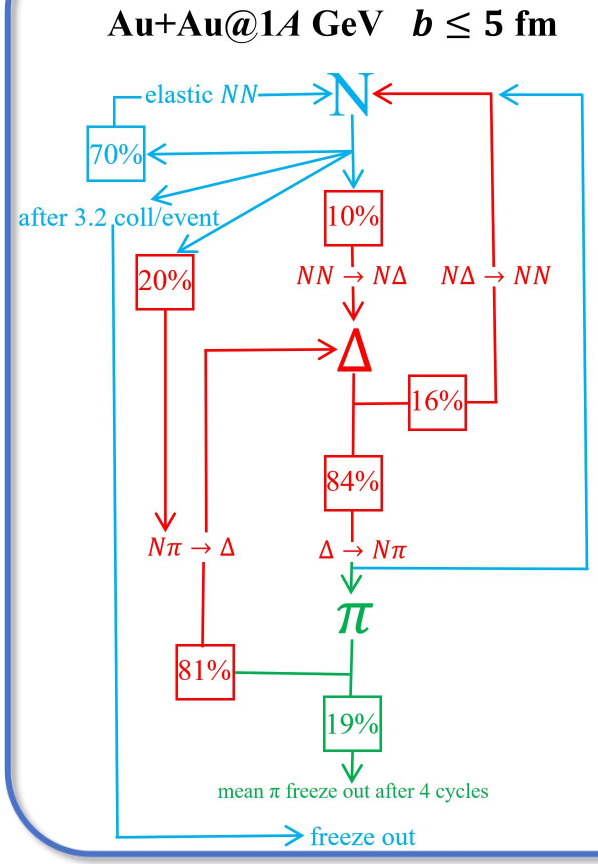


- Pion-related observables (π^-/π^+, HBT Cor., etc.) in HICs are sensitive probe of EoS at suprasaturation densities.

1.1 Background

- HICs are complex nonequilibrium dynamic processes.
- In intermediate energy HICs, **π** are dominantly produced from the decay of **Δ** resonances formed from ***NN*** inelastic scattering in the high density regions during the collision.

Example: the N-Δ-π cycle in the IQMD model



Au+Au Collisions@ 1 GeV/nucleon:

- relevant hadronic degrees of freedom: nucleon, Δ & pion

Particle Production/Absorption:

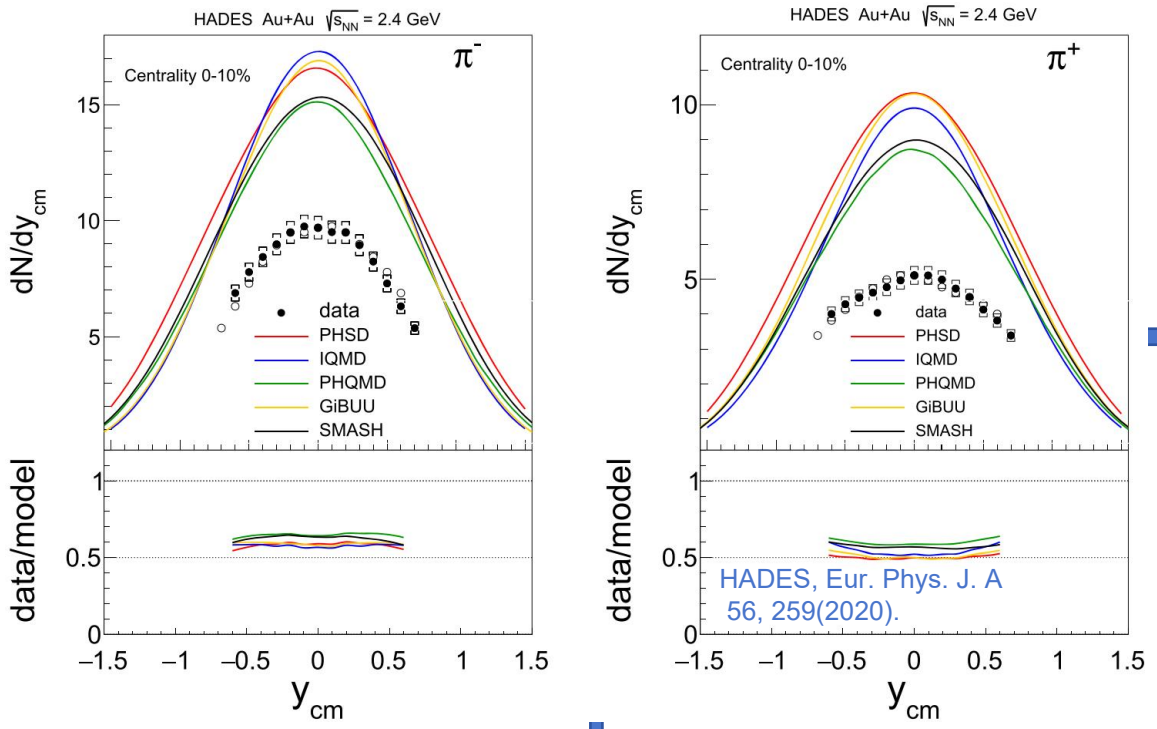
- pion production via Δ→N+π
- pion absorption requires two steps: π+N→Δ & Δ+N→N+N

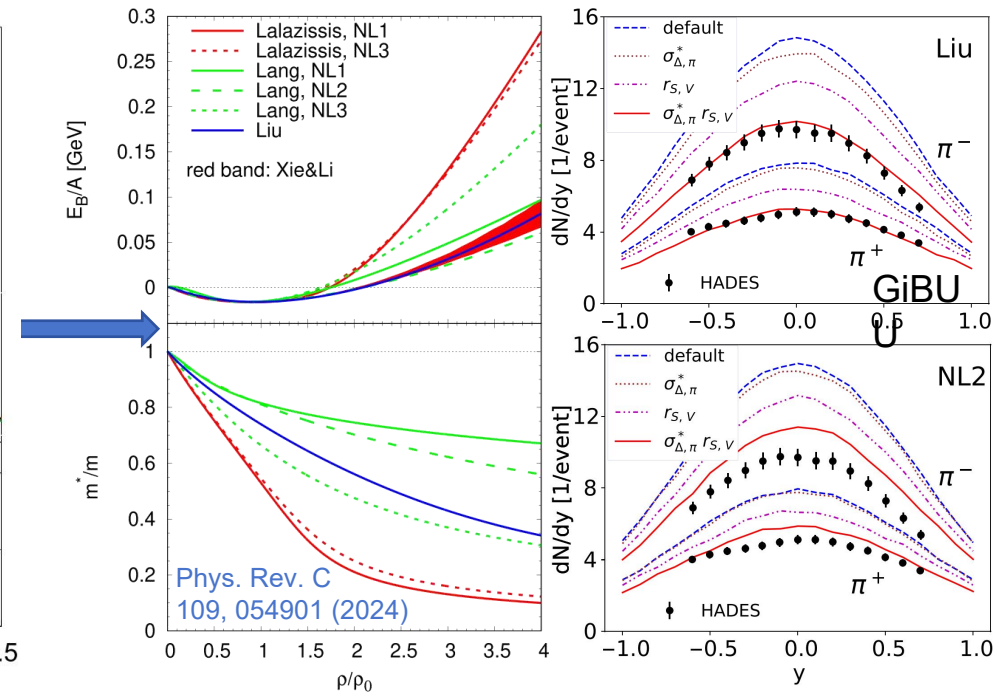
- Δ plays a crucial role in the particle production dynamics
- the average pion goes through approx. 4 Δ-cycles before freeze-out!

S. A. Bass, et al., Phys. Rev. C 51, 3343 (1995).

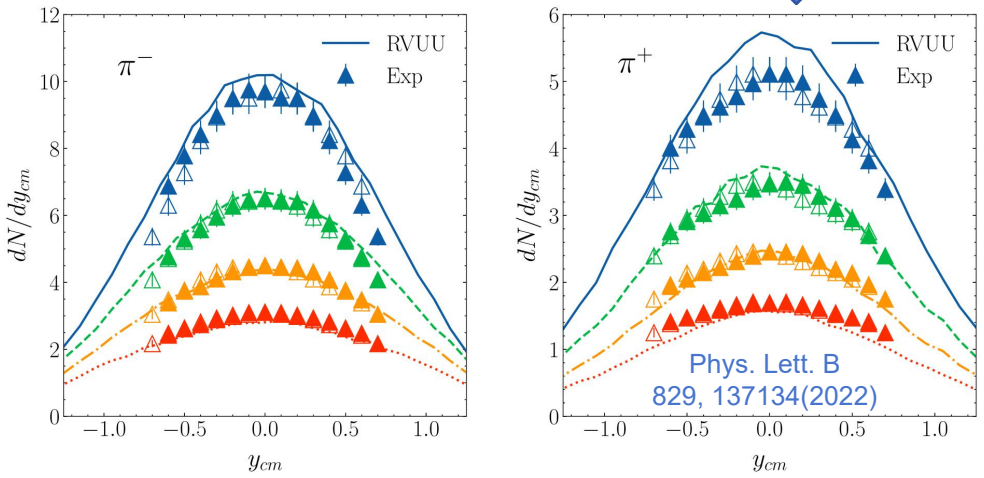
- The nuclear medium effect for resonances on the mean-field level have been studied widely and often treated in models, but in-medium effect on the cross sections are much less thoroughly investigated in the transport model calculations.

1.2 Motivation: in-medium correction on *NN* inelastic cross section





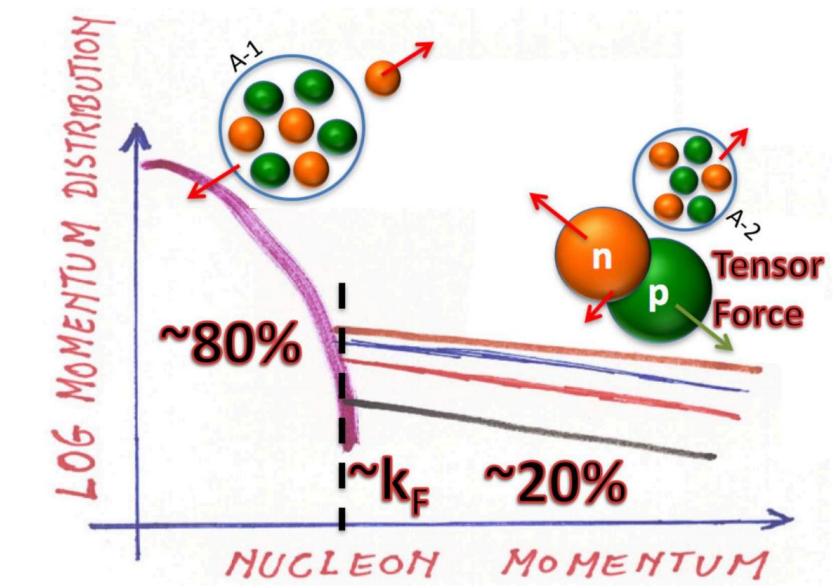
$$\sigma^*_{NN\to N\Delta}(\rho) = \sigma_{NN\to N\Delta}\, e^{-\alpha^{\pm}(\rho/\rho_0)^{3/2}}$$

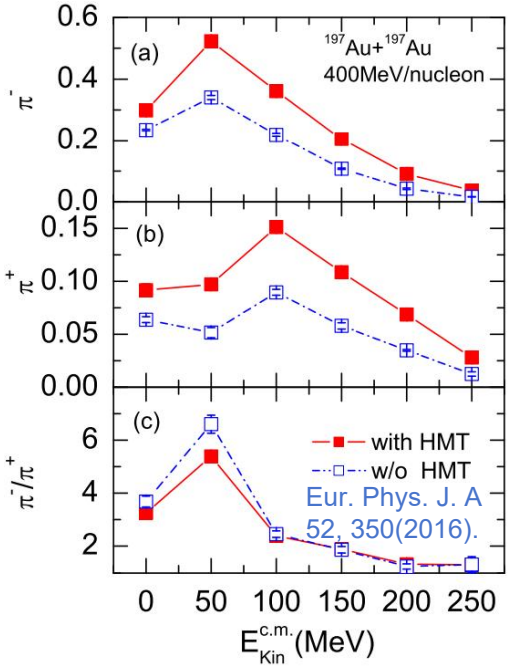


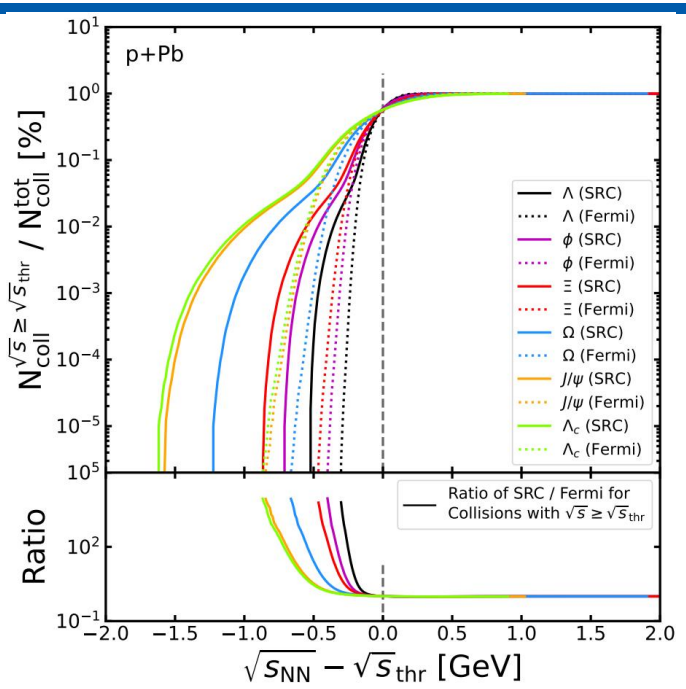
- There is a major mismatch between the charged-pion rapidity distribution calculated by various transport models and the HADES data.
- With reasonable improvements on the EoS and the in-medium modification of cross sections, theoretical calculations can describe the charged-pion yields data better.

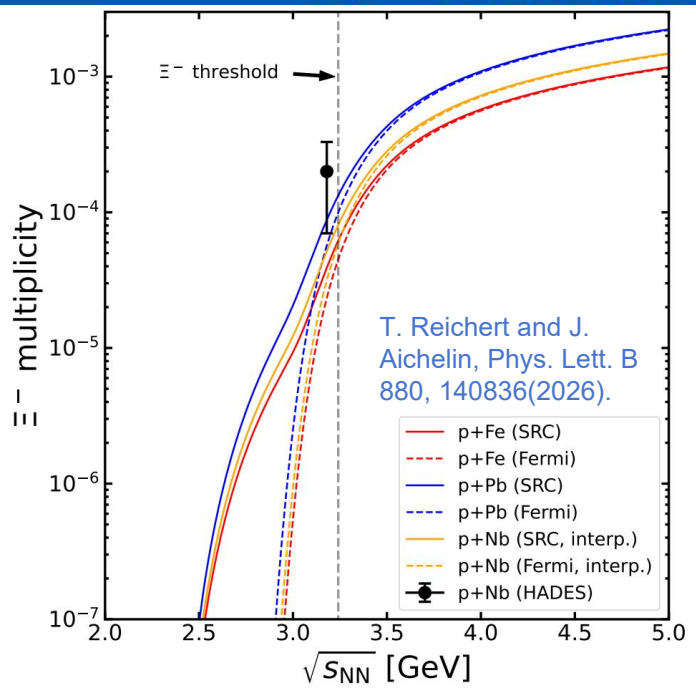
The pion production is influenced by the **EoS** and **in-medium corrections** to cross sections.

1.2 Motivation: HMT of the nucleon momentum distribution







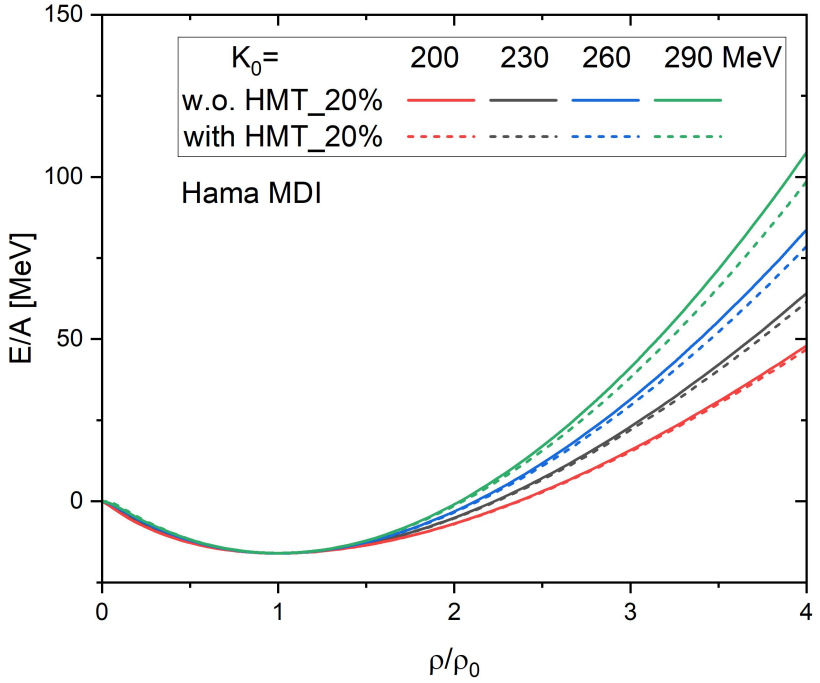


- CLAS experiments revealed that roughly 20% of nucleons in the nucleus form SRC pairs, which arise from the tensor force and the repulsive core at shorter range.
- These nucleons have a momentum distribution far above the Fermi momentum (high-momentum tail, HMT).
- HMT effect would enhance the available center of mass energy of *NN* collisions and therefore for particle production.
- The combined influence of in-medium effect and the HMT effect requires further investigation.

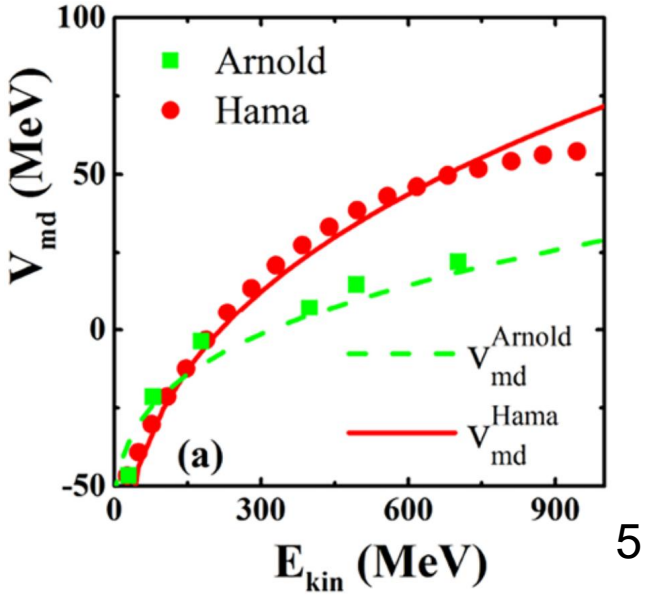
2.1 UrQMD model

- In this work, the density- and momentum-dependent potentials are adopted.
- The nucleonic potential energy *U* is calculated from the potential energy density *u*.

$$u = \frac{\alpha}{2}\frac{\rho^2}{\rho_0} + \frac{\beta}{\eta+1}\frac{\rho^{\eta+1}}{\rho_0^{\eta}} + \frac{g_{\mathrm{sur}}}{2\rho_0}(\nabla\rho)^2 + \frac{g_{\mathrm{sur,iso}}}{2}[\nabla(\rho_n-\rho_p)]^2 + t_{\mathrm{md}}\ln^2[1+a_{\mathrm{md}}(\mathbf{p}_i-\mathbf{p}_j)^2]\frac{\rho}{\rho_0} + \frac{C_s}{2}(\frac{\rho}{\rho_0})^{\gamma}\rho\delta^2.$$



Here, $\alpha = -211$ MeV, $\beta = 113$ MeV, $\eta = 1.35$, $t_{md} = 3.058$ MeV, $a_{md} = 500\ c^2/\mathrm{GeV}^2$, $C_s/2 = 20$ MeV, and $\gamma = 0.5$ are adopted, which correspond to a soft momentum-dependent EoS with an incompressibility of $K_0 = 230$ MeV, the slope of the symmetry energy $L = 54$ MeV. Both K_0 and L lie in the commonly accepted range constrained by nuclear experiments and neutron-star observations [4, 51, 52].

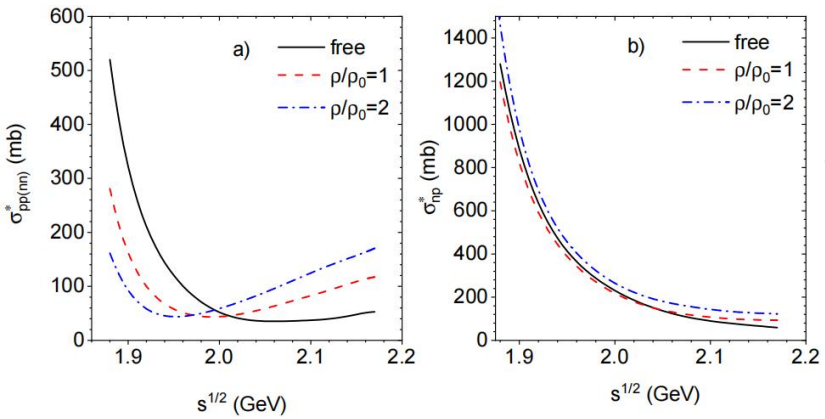


Q. F. Li, et al., Phys. Rev. C 83, 044617 (2011),
Y. J. Wang, et al., Phys. Lett. B 802, 135249 (2020),
Y. Y. Liu, et al., Phys. Rev. C 103, 014616 (2021),
P. C. Li, et al., Phys. Lett. B 828, 137019 (2022).

2.1 in-medium *NN* elastic cross section in UrQMD

➢ In-medium *NN* elastic cross sections

- The in-medium *NN* elastic scattering cross sections were calculated based on the quantum hadrodynamics (QHD) model and the Skyrme interaction with closed-time Green's function technique.



Phys. Rev. C 62, 014606(2000)
Phys. Rev. C 69, 017601(2004)
J. Phys. G 32,407–415 (2006).

- In the UrQMD model $\sigma_{\mathrm{el}}^{\mathrm{in-med.}} = F_u^p F_\alpha^p \cdot \sigma_{\mathrm{el}}^{\mathrm{free}}$,

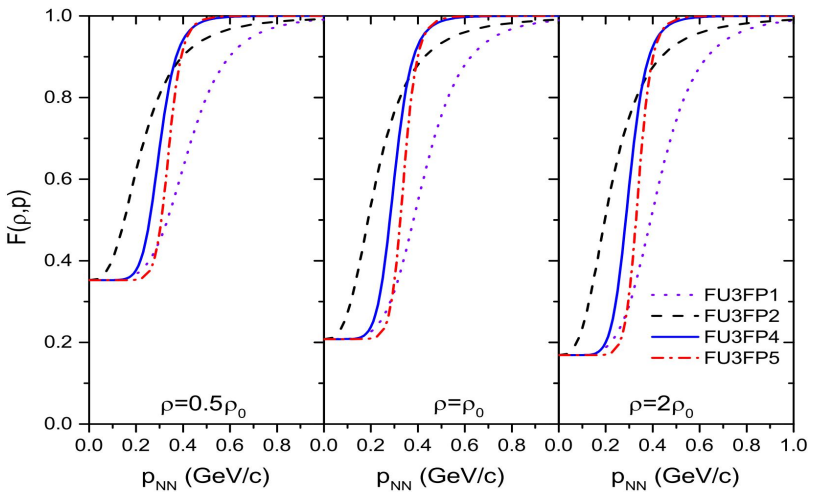
$$F_u^p = \begin{cases} f_0, & p_{NN} > 1\mathrm{GeV}/c, \\ \frac{F(u,\alpha)-f_0}{1+(p_{NN}/p_0)^\kappa} + f_0, & p_{NN} \le 1\mathrm{GeV}/c, \end{cases}$$

$$F_\alpha^p = \frac{F_\alpha - f_0}{1+\left(p_{NN}/p_0\right)^\kappa} + f_0.$$

$$F(u,\alpha) = \lambda + (1-\lambda)e^{-\frac{\rho}{\zeta\rho_0}},$$

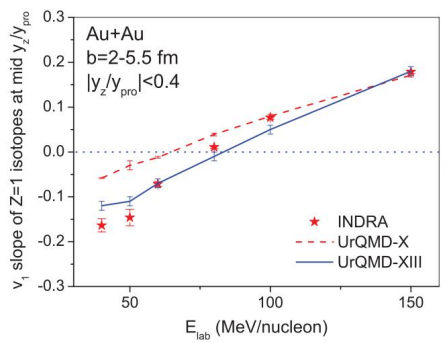
$$\text{Dirac: } F_\alpha = 1 + \tau_{ij}\frac{0.85}{1+3.25u}\alpha,$$

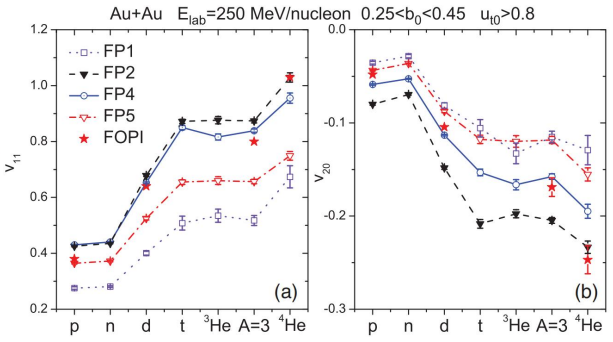
$$\text{DBHF: } F_\alpha = 1 - \tau_{ij}\frac{0.85}{1+3.25u}\alpha,$$

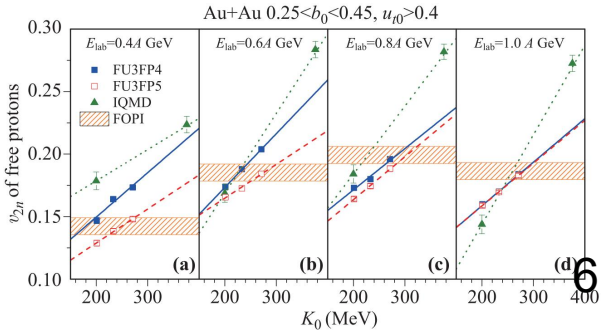


J. Phys. G 32,407–415 (2006).
Phys. Rev. C 83, 044617(2011).
Phys. Rev. C 89, 044603(2014).
Phys. Rev. C 97, 044620(2018).
Front. Phys. 15, 44302(2020).
Phys. Lett. B 802, 135249(2020)

- Collective flow and nuclear stopping data of light charged particles can be well reproduced. By comparing the data and the UrQMD calculations, **K_0=220±40 MeV**, **L=43±20 MeV** is extracted.



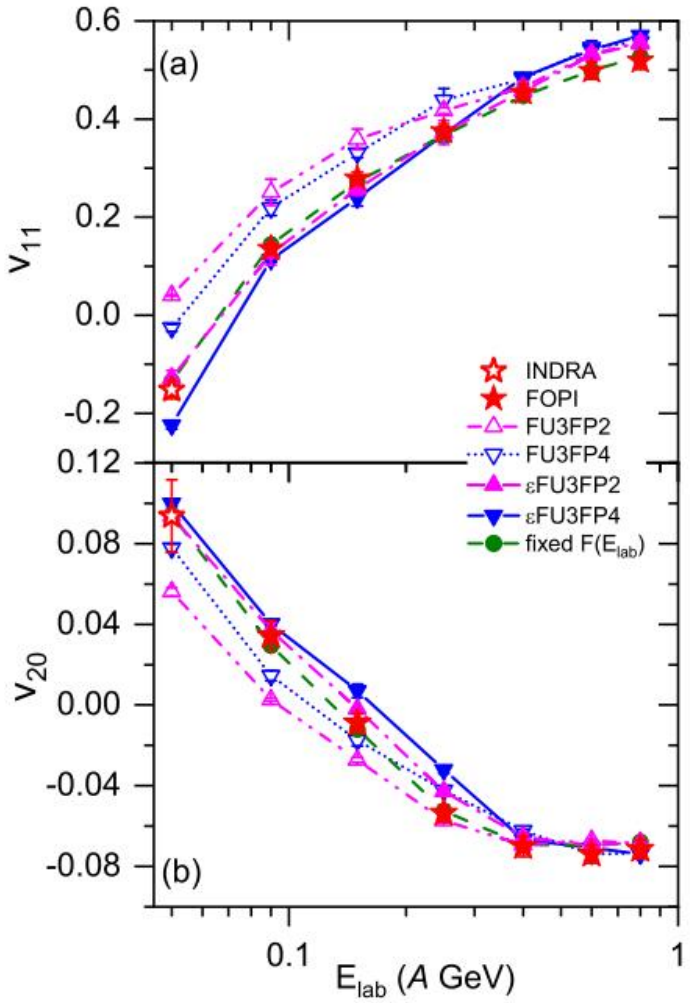


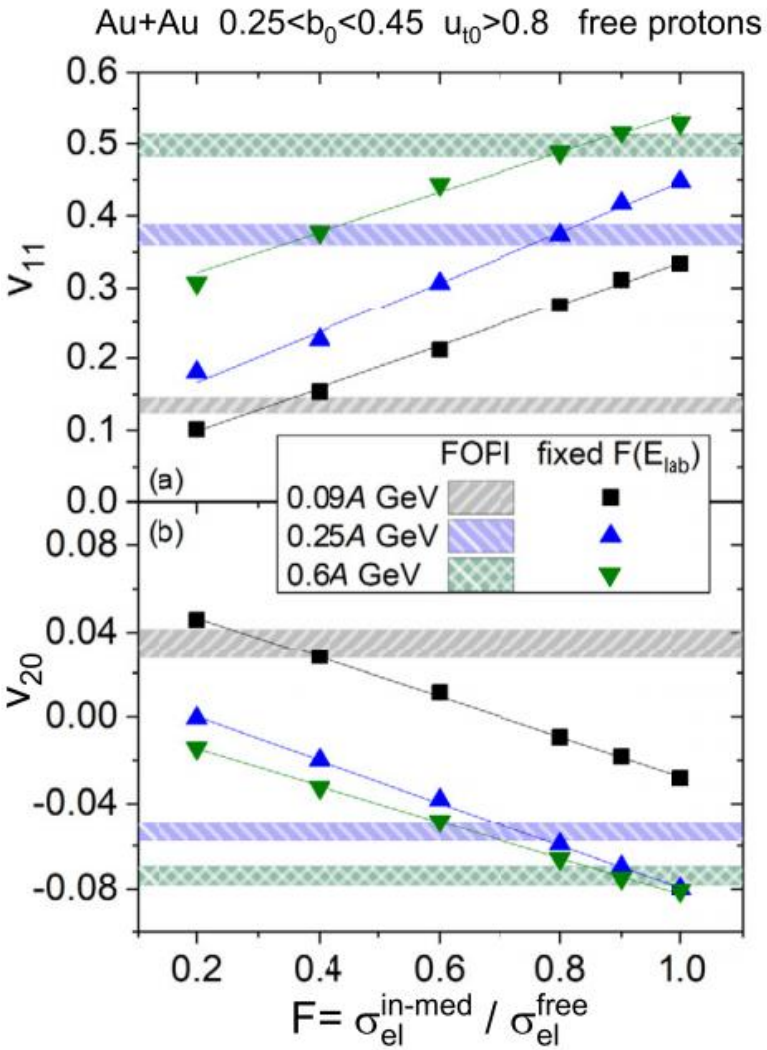


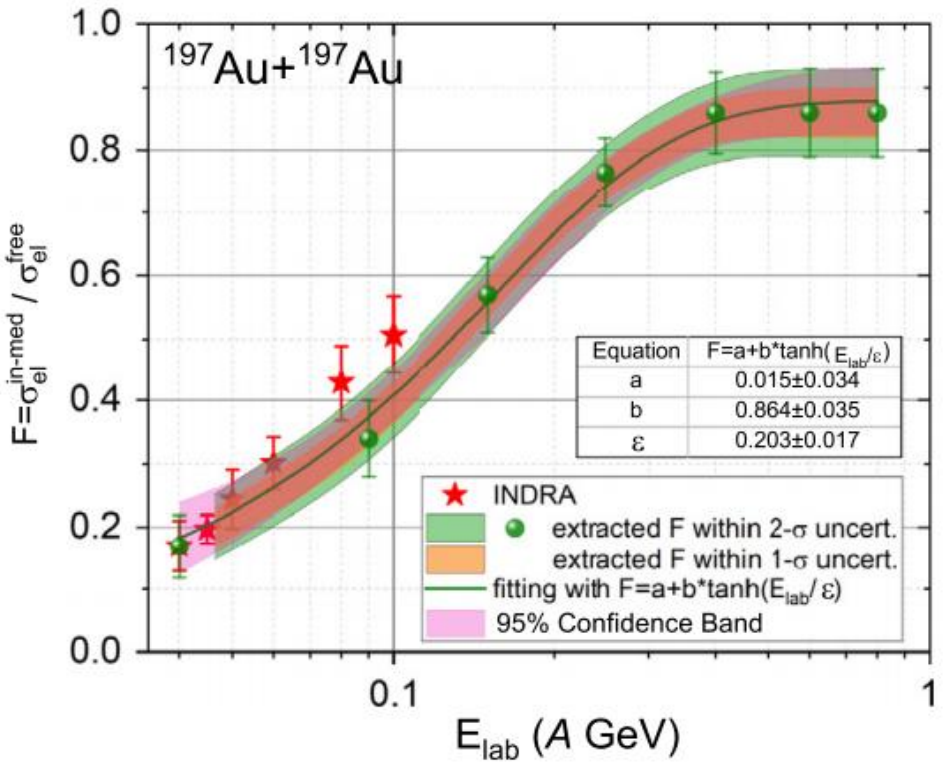
2.1 in-medium *NN* elastic cross section in UrQMD

- In-medium *NN* elastic cross sections

The beam energy dependent in-medium correction factor also can be deduced from the comparison of the excitation functions of the directed, elliptic flow and nuclear stopping between the calculated results and the FOPI experimental data.







P. C. Li, et al., Phys. Lett. B 828, 137019(2022).

2.1 in-medium *NN* inelastic cross section

➢ Within the framework of the relativistic BUU approach, by introducing the σ, ω, ρ, δ meson exchange into the effective Lagrangian and adopting the density-dependent or nonlinear-dependent coupling constants, energy-, density-, isospin-, and temperature-dependent *NN* inelastic cross sections were calculated.

- The effective Lagrangian $\mathcal{L} = \mathcal{L}_F + \mathcal{L}_I$.
- The free Lagrangian density

$$\begin{aligned}\mathcal{L}_F =& \bar{\Psi}\left[i\gamma_\mu\partial^\mu - m_N\right]\Psi + \bar{\Psi}_{\Delta\nu}\left[i\gamma_\mu\partial^\mu - m_\Delta\right]\Psi^\nu_\Delta \\ &+ \frac{1}{2}\partial_\mu\sigma\partial^\mu\sigma + \frac{1}{2}\partial_\mu\vec{\delta}\partial^\mu\vec{\delta} - \frac{1}{4}F_{\mu\nu}\cdot F^{\mu\nu} - \frac{1}{4}\vec{L}_{\mu\nu}\cdot\vec{L}^{\mu\nu} \\ &- \frac{1}{2}m_\sigma^2\sigma^2 - \frac{1}{2}m_\delta^2\vec{\delta}^2 + \frac{1}{2}m_\omega^2\omega_\mu\omega^\mu + \frac{1}{2}m_\rho^2\vec{\rho}_\mu\vec{\rho}^\mu \\ &- U_{NL}(\sigma,\omega^\mu,\vec{\delta},\vec{\rho}^\mu),\end{aligned}$$

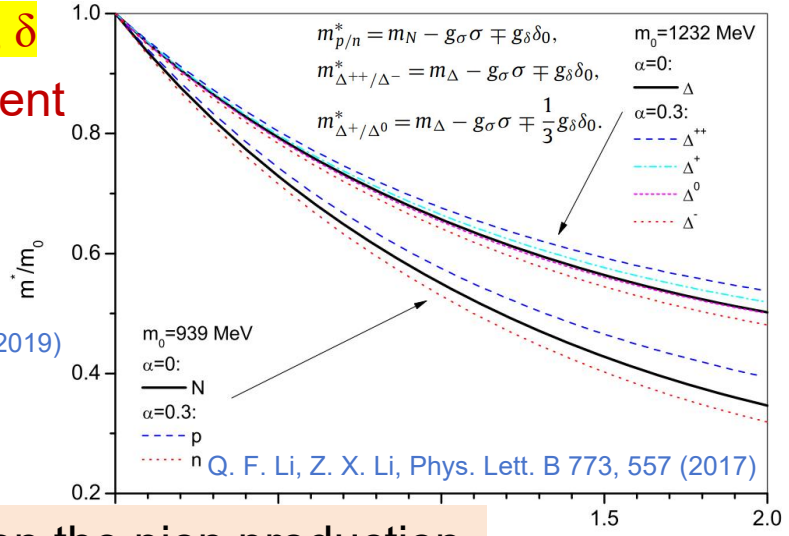
- The nonlinear potential associated with meson–meson couplings(omitted for density-dependent nucleon–meson couplings case),

$$\begin{aligned}U_{NL}(\sigma,\omega^\mu,\vec{\delta},\vec{\rho}^\mu) =& \frac{1}{3}g_2\sigma^3 + \frac{1}{4}g_3\sigma^4 \\ &-\Lambda_s(g_{NN}^{\sigma\,2}\sigma^2)(g_{NN}^{\delta\,2}\vec{\delta}^2) \\ &-\Lambda_\nu(g_{NN}^{\omega\,2}\omega_\mu\omega^\mu)(g_{NN}^{\rho\,2}\vec{\rho}_\mu\cdot\vec{\rho}^\mu).\end{aligned}$$

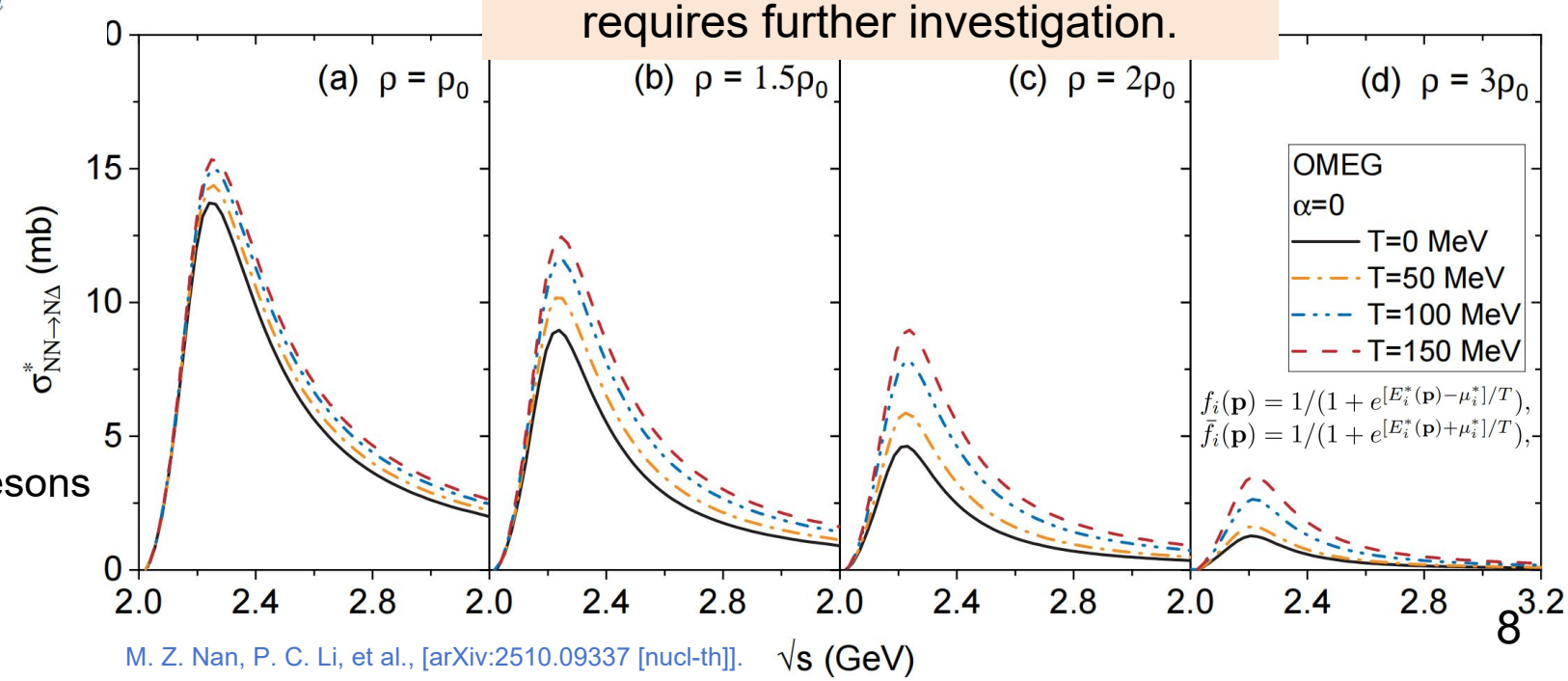
- The interaction part of baryons coupled to mesons

$$\begin{aligned}\mathcal{L}_I =& g_{NN}^\sigma\bar{\Psi}\Psi\sigma + g_{NN}^\delta\bar{\Psi}\vec{\tau}\cdot\Psi\vec{\delta} - g_{NN}^\omega\bar{\Psi}\gamma_\mu\Psi\omega^\mu \\ &- g_{NN}^\rho\bar{\Psi}\gamma_\mu\vec{\tau}\cdot\Psi\vec{\rho}^\mu + g_{\Delta\Delta}^\sigma\bar{\Psi}_\Delta\Psi_\Delta\sigma + g_{\Delta\Delta}^\delta\bar{\Psi}_\Delta\vec{\tau}\cdot\Psi_\Delta\vec{\delta} \\ &- g_{\Delta\Delta}^\omega\bar{\Psi}_\Delta\gamma_\mu\Psi_\Delta\omega^\mu - g_{\Delta\Delta}^\rho\bar{\Psi}_\Delta\gamma_\mu\vec{\tau}\cdot\Psi_\Delta\vec{\rho}^\mu,\end{aligned}$$

Q. F. Li, et al., Phys. Lett. B 773, 557(2017).
Q. F. Li, et al., Sci. China-Phys. Mech. Astron. 62, 972011(2019)
M. Z. Nan, et al., Eur. Phys. J. A 60, 131(2024).
M. Z. Nan, et al., Chin. Phys. C 49, 094112(2025).
M. Z. Nan, et al., arXiv:2510.09337



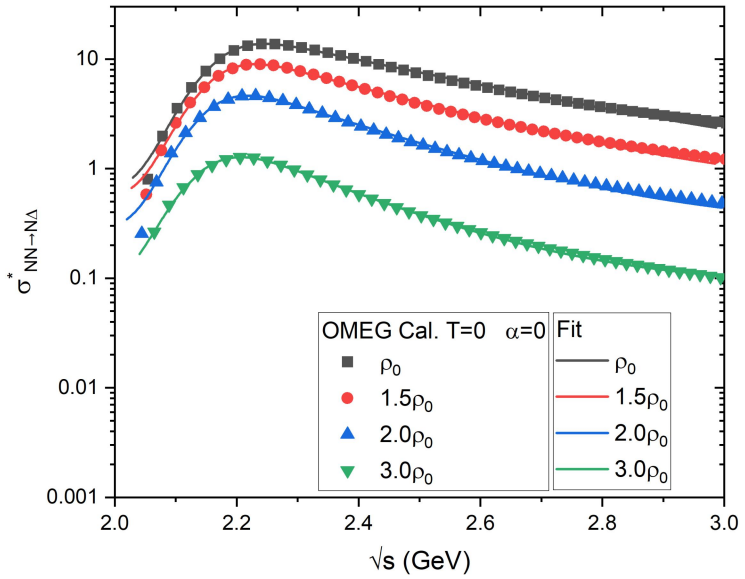
The influence on the pion production requires further investigation.



M. Z. Nan, P. C. Li, et al., [arXiv:2510.09337 [nucl-th]].

2.1 in-medium *NN* inelastic cross section in UrQMD

- In-medium *NN* inelastic cross sections



$$\sigma^*_{NN\to N\Delta}(\sqrt{s}) = \begin{cases} 3.85\exp\left[-\dfrac{(\sqrt{s}-2.121)^2}{0.0024}\right], & \text{for} \quad \sqrt{s}\le 2.10, \\ 1.262 + 17.792\exp\left(0.015 - \dfrac{\sqrt{s}-2.163}{0.314}\right) & \\ \quad \cdot\dfrac{1+\mathrm{erf}(z/\sqrt{2})}{2}, & \text{for } \sqrt{s} > 2.10, \end{cases}$$

with

$$z = \frac{\sqrt{s}-2.163}{0.055} - 0.175.$$

$$F_\rho(u) = 2.68\exp\left(-\frac{u}{1.16}\right) - 0.126, \quad u = \frac{\rho}{\rho_0}.$$

$$\sigma^{\text{in}}_{NN\to N\Delta}(\sqrt{s},\rho) = C_{\text{iso}}\sigma^*_{NN\to N\Delta}(\sqrt{s})F_\rho(u),$$

- In-medium shift of the production threshold

T. Song and C. M. Ko, Phys. Rev. C 91(2015), 014901

$$\sqrt{s}_{\text{th}} = \sqrt{\left(m_3^* + \Sigma_3^0 + m_4^* + \Sigma_4^0\right)^2 - |\mathbf{\Sigma}_3 + \mathbf{\Sigma}_4|^2}.$$

$$\sqrt{s}_{\text{in}} - \sqrt{s}_{\text{th}} \simeq E_1^* + E_2^* + \Sigma_1^0 + \Sigma_2^0 - m_3^* - m_4^* - \Sigma_3^0 - \Sigma_4^0,$$

$$\sqrt{s}_{\text{in}} - \sqrt{s}_{\text{th}} \simeq m_1 + m_2 - m_3 - m_4 + \Sigma_1^s + \Sigma_2^s - \Sigma_3^s - \Sigma_4^s + \frac{|\mathbf{p}_1^*|^2}{2m_1^*} + \frac{|\mathbf{p}_2^*|^2}{2m_2^*} + \Sigma_1^0 + \Sigma_2^0 - \Sigma_3^0 - \Sigma_4^0$$

A reduced RMF-like prescription for the $NN \to N\Delta$ threshold is employed here. For a baryon B, the scalar and vector self-energies are parametrized as

$$\Sigma_{s,B} = x_{s,B}\,(C_1 + C_2\tau_B\delta)\,u^{C_5}$$
$$\Sigma_{0,B} = x_{0,B}\,(C_3 + C_4\tau_B\delta)\,u^{C_5}$$

where $u = \rho/\rho_0$, $\delta = (\rho_n - \rho_p)/(\rho_n + \rho_p)$, and τ_B is the reduced isospin factor of baryon B. In the present convention, $\tau_p = \tau_{\Delta^{++}} = 1$, $\tau_n = \tau_{\Delta^-} = -1$, $\tau_{\Delta^+} = 1/3$, and $\tau_{\Delta^0} = -1/3$. For nucleons, $x_{s,N} = x_{0,N} = 1$, while for Δ resonances the reduced couplings are taken as $x_{s,\Delta} = x_{0,\Delta} = 2/3$, motivated by the reduced Δ potential $U_\Delta \simeq (2/3)U_N$ discussed in Ref. [29].

$$C_1 = -0.350 \text{ GeV and } C_3 = 0.300 \text{ GeV}$$
$$C_2 = 0.035 \text{ GeV and } C_4 = -0.068 \text{ GeV}$$

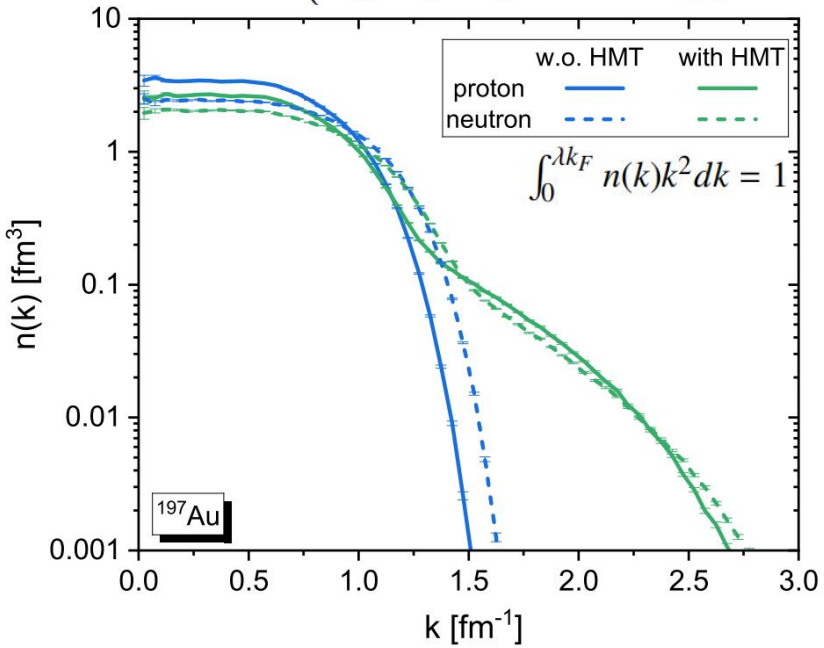
P. C. Li, et al., [arXiv:2609.25818 [nucl-th]].

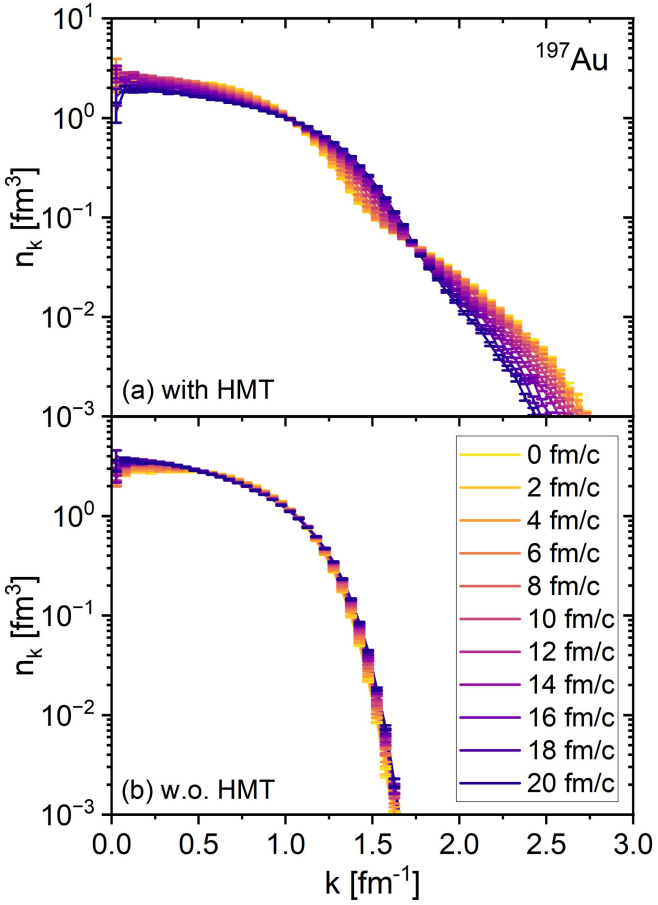
2.1 HMT in UrQMD

- To include the SRC-induced HMT, a momentum distribution extending up to λk_F is used, with the cutoff parameter set to λ=2.2. The fraction of nucleons in the HMT is taken as $P_{HMT} = 0.2$.
- The introduction of the HMT will increase the average kinetic energy of the initialized nuclear system. To avoid mixing the physical HMT effect with an artificial change of the nuclear EoS, the potential parameters are refitted.
- The stability of the initialized nuclei is further examined.

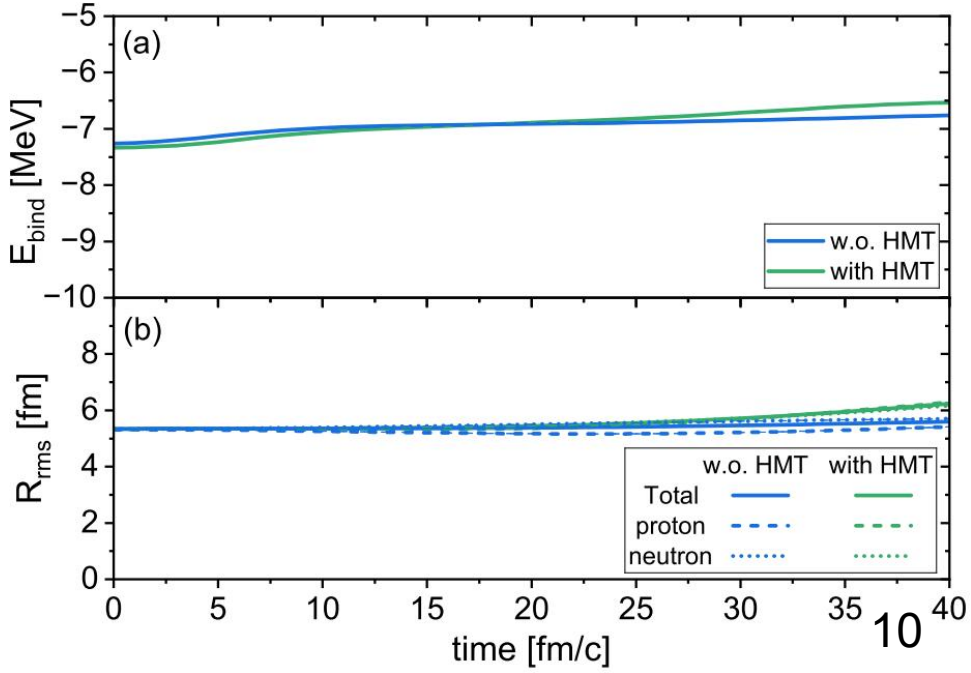
The momentum distribution used in the initialization is

$$n(k) = \begin{cases} C_1, & 0 < k < k_F, \\ C_2/k^4, & k_F < k < \lambda k_F, \end{cases}$$

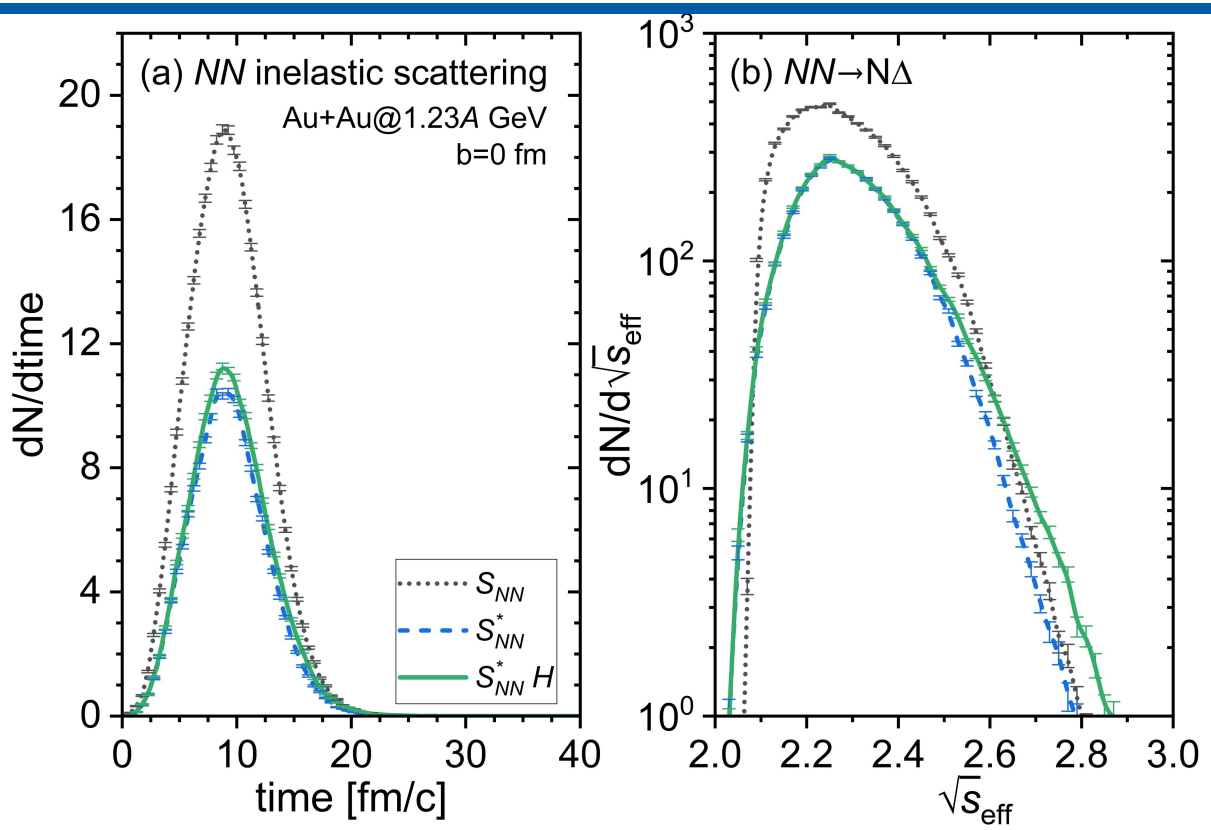


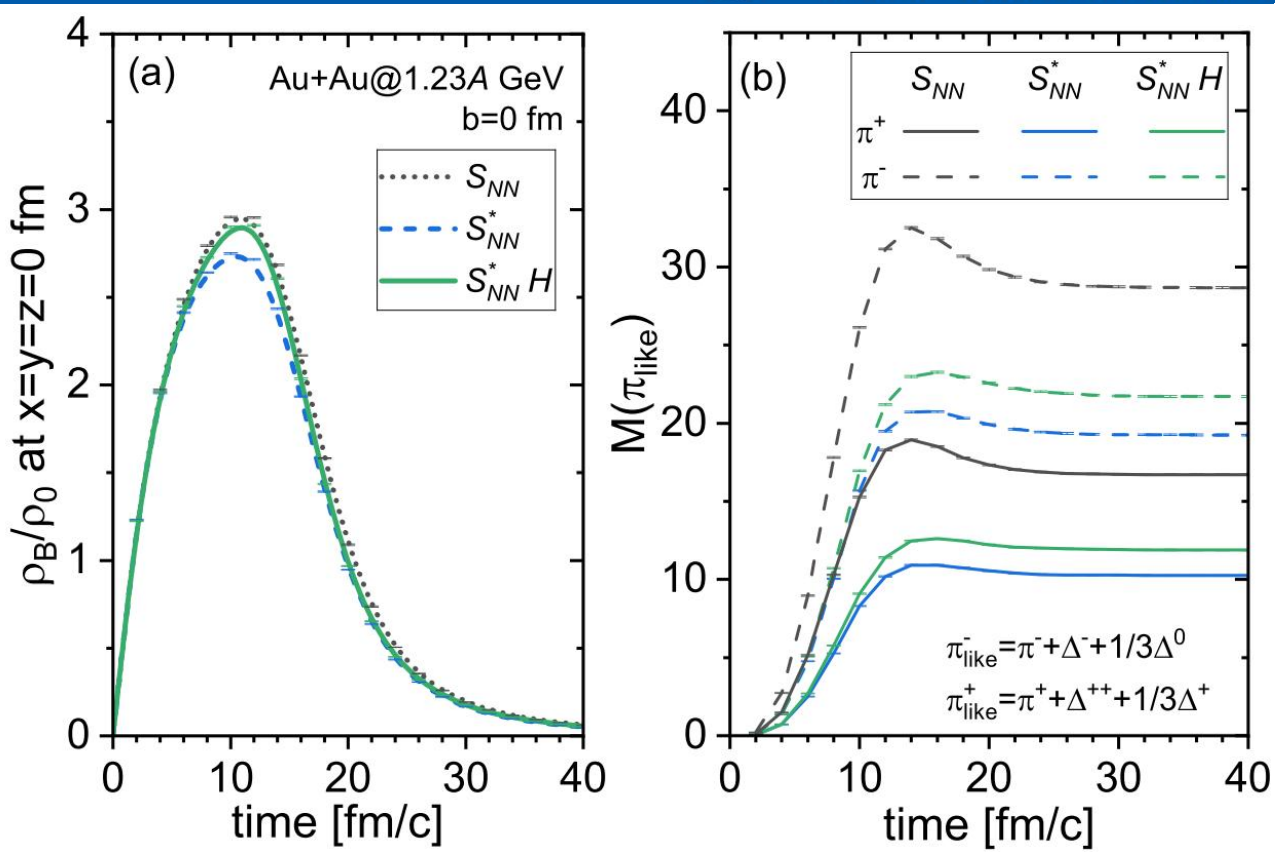


HMT	K_0 (MeV)	α (MeV)	β (MeV)	η
w.o.	230	-211	113	1.35
with	230	-325	200	1.22



3.1 Results and discussion: dynamical reaction process



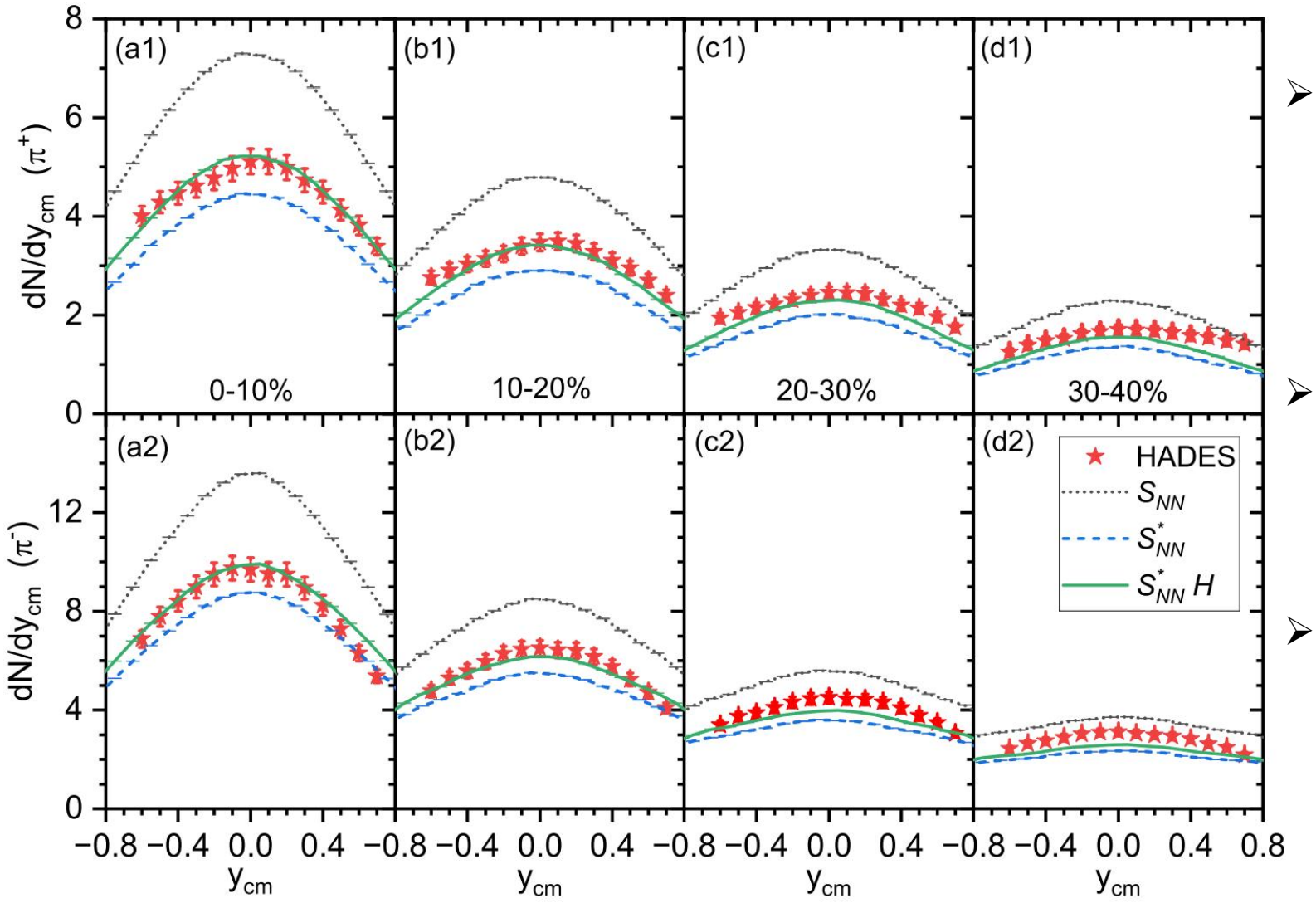


- In-medium reduced $NN \rightarrow N\Delta$ cross section leads to less stopping and, thus, to a lower central density.
- The HMT increases the rate of $NN \rightarrow N\Delta$ collisions, which results in more stopping and higher central density.

S_{NN}: free *NN* inelastic cross sections
S^*_{NN}: in-medium *NN* inelastic cross sections
$S^*_{NN}H$: in-medium *NN* inelastic cross sections combined with the HMT effect

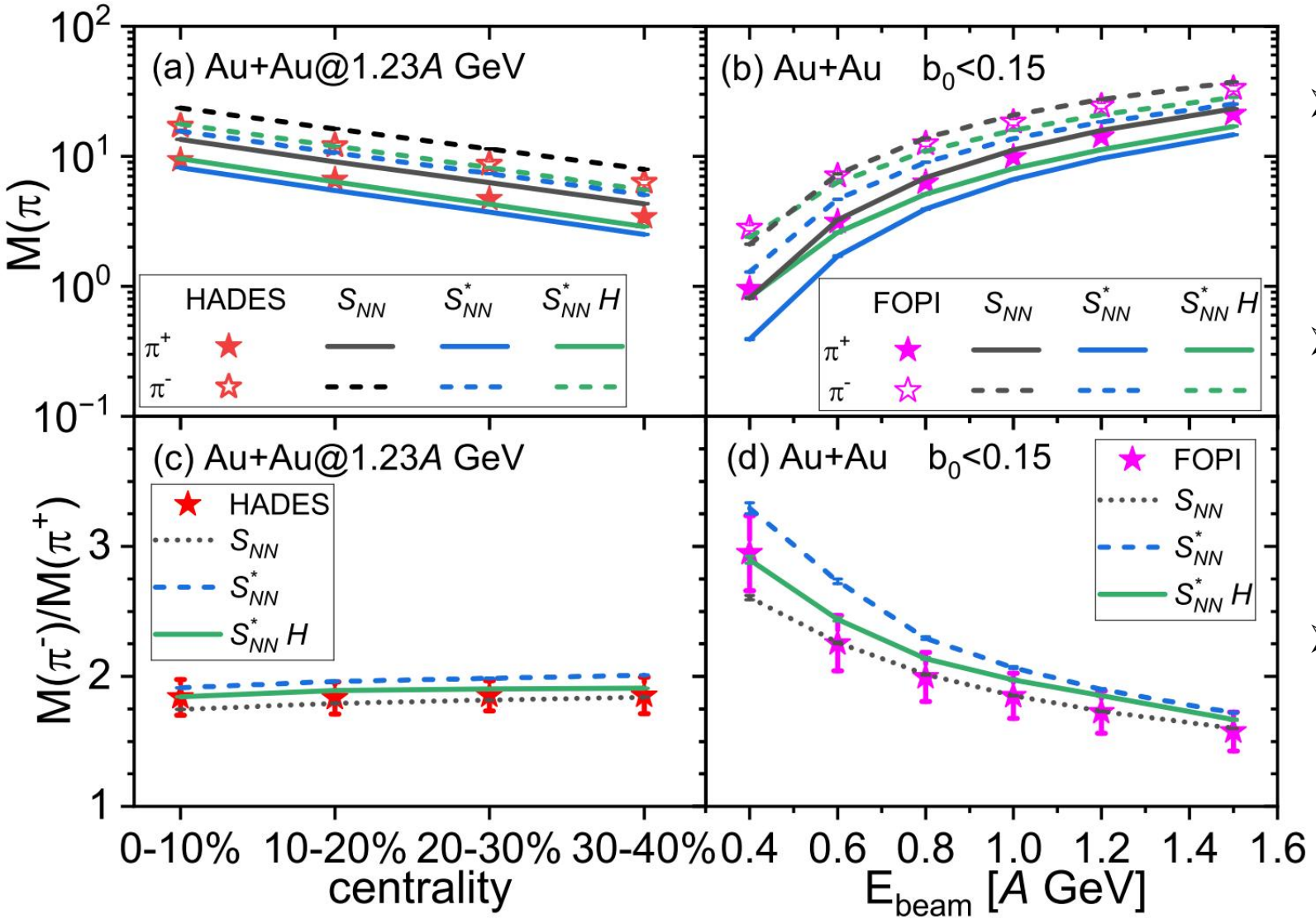
- The in-medium effect suppresses pion production, whereas the HMT effect partly restores the pion yield by increasing the available energy in *NN* inelastic collisions.

3.2 Results and discussion: rapidity distribution



- The calculation without the in-medium correction of *NN* inelastic cross sections clearly **overestimates** the pion rapidity distributions for both charge states.
- After the in-medium $NN \rightarrow N\Delta$ cross section is introduced, the pion rapidity distributions are strongly **suppressed**.
- When the HMT is further included, the pion rapidity distributions are **enhanced** again and move closer to the experimental data.

3.3 Results and discussion: total yields



- In-medium inelastic cross section and the HMT affect pion production in opposite directions.
- The in-medium modification of the inelastic channel does not suppress π−and π+ production in exactly the same way.
- The HMT lowers the ratio relative to the calculation without the HMT because the recovery of π+ production is slightly stronger than that of π− production.

4 Summary and outlook

- ✓ The in-medium *NN* inelastic cross sections and the SRC-induced HMT of the nucleon momentum distribution are introduced into the UrQMD model to investigate pion production in intermediate-energy HICs.
- ✓ The in-medium correction of the $NN \to N\Delta$ cross section suppresses pion production by reducing the probability of resonance production in dense matter, whereas the HMT partly restores the pion yield by increasing the high-momentum components of nucleons and the available energy in early *NN* collisions.
- ✓ With the simultaneous inclusion of these two effects, the rapidity distributions, transverse-momentum spectra, centrality dependence, beam-energy dependence, and charged-pion ratios can be better described.
- ✓ These results indicate that both the in-medium correction of *NN* inelastic cross sections and the initial high-momentum components are important for a consistent description of pion production.

- First, the HMT initialization would be further constrained by nuclear-structure information. (ongoing)
- Second, the density and isospin dependence of the in-medium *NN* inelastic cross section would be improved. (finished)
- Third, a more self-consistent treatment of the single-particle potential, in-medium cross section, and the threshold effect would be conducted within the same relativistic framework. (ongoing)

Thank you for your attention!

P. C. Li gratefully acknowledges the warm hospitality of BLTP, JINR, during the last three months (Jul.-Oct. 2026).

Another work completed during the visit to BLTP



Short communication ● Open access Under a Creative Commons license ↗ Get rights and content ↗

Letter

Dynamical Coulomb effects on charged-pion HBT-radius splitting in central Au+Au collisions at few-GeV energies

Pengcheng Li [a,b], Yongjia Wang [a], Qingfeng Li [a]

[a] School of Science, Huzhou Normal University, 313000, Huzhou, China

[b] Bogoliubov Laboratory of Theoretical Physics, Joint Institute for Nuclear Research, 141980, Dubna, Russia

Physics Letters B

Date: Available online 19 October 2026

Article: 141081

In Press, Journal Pre-proof

View accessibility information

Published by

ELSEVIER

New **Are you looking for collaborators?**

Discover researchers and experts working in your field of interes

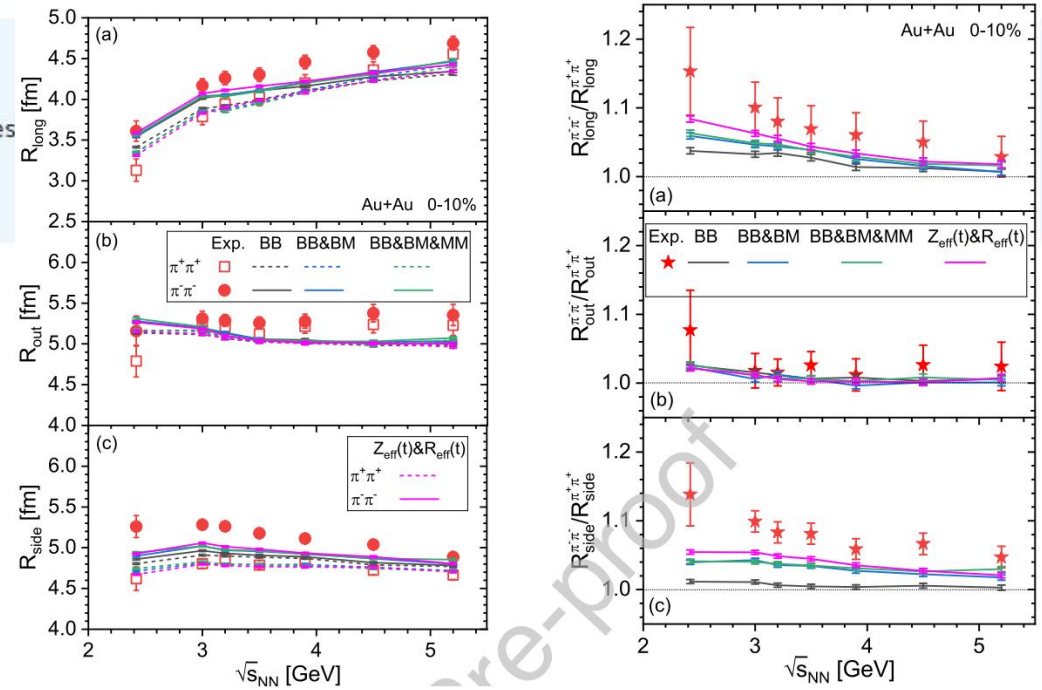
Try LeapSpace ↗

Available online 19 October 2026.

What do these dates mean?

Editor: Baha Balantekin

Show less



Pre-proof

P. C. Li gratefully acknowledges the warm hospitality of BLTP, JINR during the last three months (Jul.-Oct. 2026).

Back up

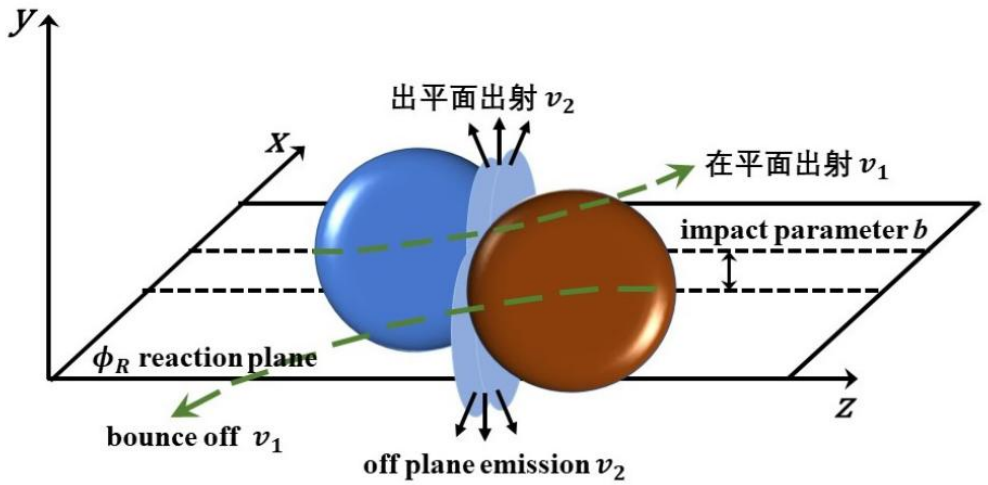
Back up：Collective flows and nuclear stopping

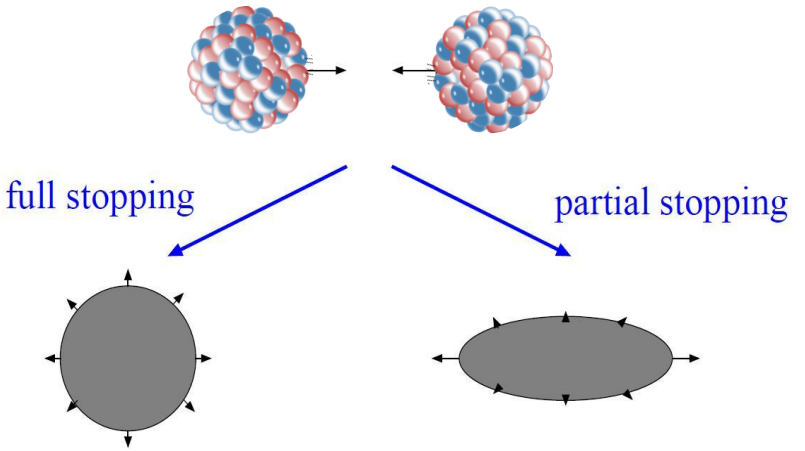
$$E\frac{d^3N}{d^3p} = \frac{d^3N}{p_T dp_T dy d\phi} = \frac{1}{2\pi}\frac{d^2}{p_T dp_T dy}\left\{1 + \sum_{n=1}^{\infty} 2v_n \cos[n(\phi - \Psi_n)]\right\}.$$

$$v_n = \langle \cos[n(\phi - \Psi_R)]\rangle = \langle \cos(n\phi)\rangle.$$

$$v_1 = \langle \cos(\phi)\rangle = \left\langle \frac{p_x}{p_t} \right\rangle,$$

$$v_2 = \langle \cos(2\phi)\rangle = \left\langle \frac{p_x^2 - p_y^2}{p_t^2} \right\rangle$$





$$R_E = \frac{\sum E_\perp}{2\sum E_\parallel}$$

$$vartl = \frac{\langle y_x^2 \rangle}{\langle y_z^2 \rangle}$$

$$\langle y_{x,z}^2 \rangle = \frac{\sum (y_{x,z}^2 N_{y_{x,z}})}{\sum N_{y_{x,z}}}$$

Back up: NN inelastic cross section

$$\begin{aligned}\mathcal{L}_F =&\bar{\Psi}\left[i\gamma_\mu\partial^\mu - m_N\right]\Psi + \bar{\Psi}_{\Delta\nu}\left[i\gamma_\mu\partial^\mu - m_\Delta\right]\Psi^\nu_\Delta \\ &+\frac{1}{2}\partial_\mu\sigma\partial^\mu\sigma + \frac{1}{2}\partial_\mu\vec{\delta}\partial^\mu\vec{\delta} - \frac{1}{4}F_{\mu\nu}\cdot F^{\mu\nu} - \frac{1}{4}\vec{L}_{\mu\nu}\cdot\vec{L}^{\mu\nu} \\ &-\frac{1}{2}m_\sigma^2\sigma^2 - \frac{1}{2}m_\delta^2\vec{\delta}^2 + \frac{1}{2}m_\omega^2\omega_\mu\omega^\mu + \frac{1}{2}m_\rho^2\vec{\rho}_\mu\vec{\rho}^\mu \\ &-U_{NL}(\sigma,\omega^\mu,\vec{\delta},\vec{\rho}^\mu),\end{aligned}$$

$$\begin{aligned}\mathcal{L}_I =&g^\sigma_{NN}\bar{\Psi}\Psi\sigma + g^\delta_{NN}\bar{\Psi}\vec{\tau}\cdot\Psi\vec{\delta} - g^\omega_{NN}\bar{\Psi}\gamma_\mu\Psi\omega^\mu \\ &-g^\rho_{NN}\bar{\Psi}\gamma_\mu\vec{\tau}\cdot\Psi\vec{\rho}^\mu + g^\sigma_{\Delta\Delta}\bar{\Psi}_\Delta\Psi_\Delta\sigma + g^\delta_{\Delta\Delta}\bar{\Psi}_\Delta\vec{\tau}\cdot\Psi_\Delta\vec{\delta} \\ &-g^\omega_{\Delta\Delta}\bar{\Psi}_\Delta\gamma_\mu\Psi_\Delta\omega^\mu - g^\rho_{\Delta\Delta}\bar{\Psi}_\Delta\gamma_\mu\vec{\tau}\cdot\Psi_\Delta\vec{\rho}^\mu,\end{aligned}$$

$$\begin{aligned}U_{NL}(\sigma,\omega^\mu,\vec{\delta},\vec{\rho}^\mu) =&\frac{1}{3}g_2\sigma^3 + \frac{1}{4}g_3\sigma^4 \\ &-\Lambda_s({g^\sigma_{NN}}^2\sigma^2)({g^\delta_{NN}}^2\vec{\delta}^2) \\ &-\Lambda_v({g^\omega_{NN}}^2\omega_\mu\omega^\mu)({g^\rho_{NN}}^2\vec{\rho}_\mu\cdot\vec{\rho}^\mu).\end{aligned}$$

- Density-dependent coupling constants DD-MEδ

  X. Roca-Maza, X. Vinas, M. Centelles, P. Ring and P. Schuck, Phys. Rev. C 84, 054309 (2011)

- Nonlinear-dependent coupling constants OMEG

  N. Zabari, S. Kubis, and W. W´ojcik, Phys. Rev. C 99, 035209 (2019) & Phys. Rev. C 100, 015808 (2019)

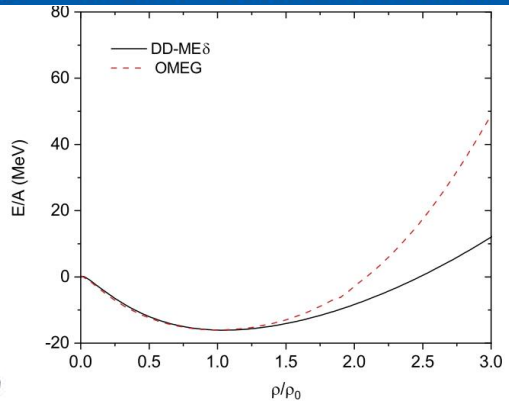
  $\Lambda_{\sigma\delta} = 50, \quad \Lambda_{\omega\rho} = 173.77$

The equation of motion of the meson fields

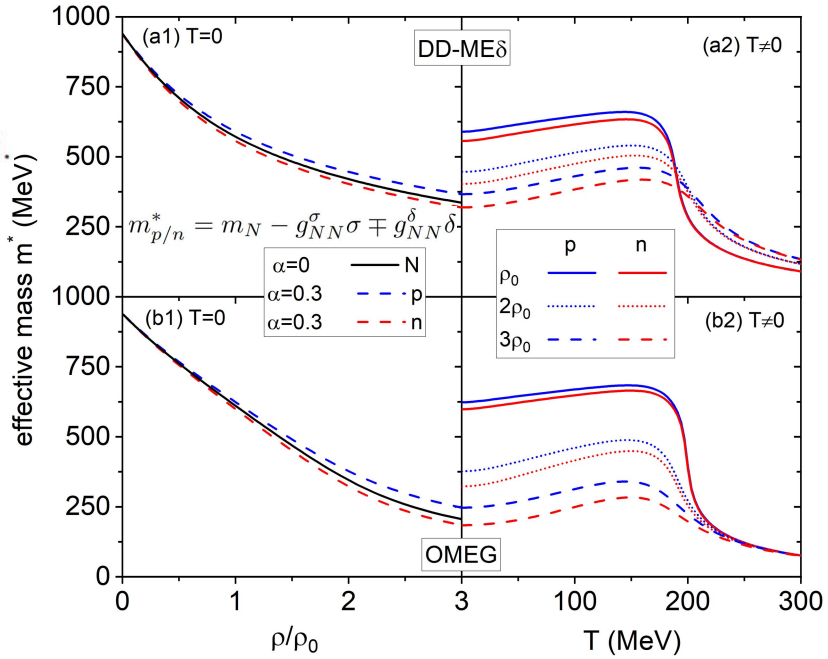
$$\begin{aligned}\left(m_\sigma^2 + g_2\sigma + g_3\sigma^2 - 2\Lambda_{\sigma\delta}\delta^2\right)\sigma &= g_\sigma\left(\rho_p^s + \rho_n^s\right), \\ \left(m_\omega^2 + 2\Lambda_{\omega\rho}\rho^2\right)\omega &= g_\omega\left(\rho_p + \rho_n\right), \\ \left(m_\delta^2 - 2\Lambda_{\sigma\delta}\sigma^2\right)\delta &= g_\delta\left(\rho_p^s - \rho_n^s\right), \\ \left(m_\rho^2 + 2\Lambda_{\omega\rho}\omega^2\right)\rho &= g_\rho\left(\rho_p - \rho_n\right).\end{aligned}$$

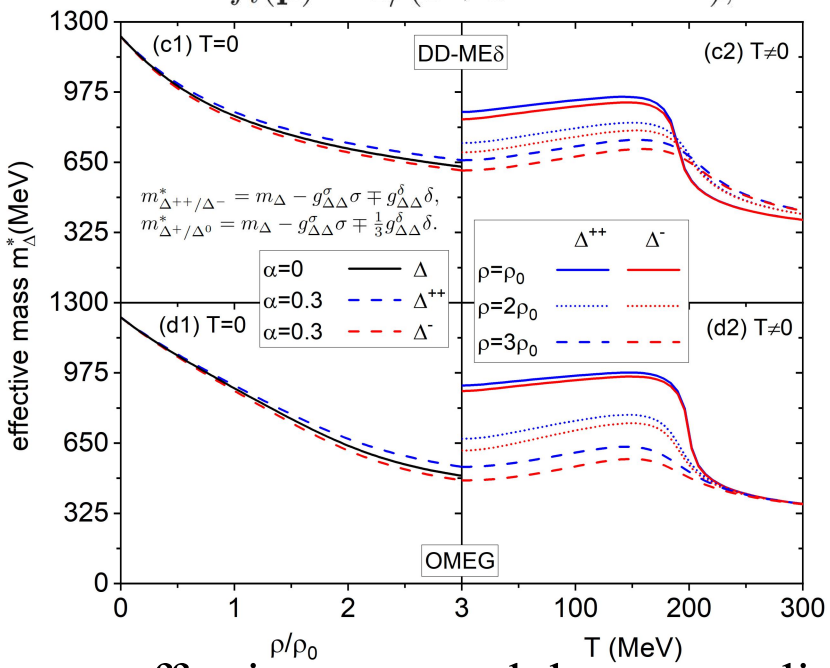
The baryon density and scalar densities

$$\rho_i = 2\int\frac{d^3\mathbf{p}}{(2\pi)^3}\left[f_i(\mathbf{p}) - \bar{f}_i(\mathbf{p})\right], \quad \rho_i^s = 2\int\frac{d^3\mathbf{p}}{(2\pi)^3}\frac{m_i^*}{E_i^*}\left[f_i(\mathbf{p}) + \bar{f}_i(\mathbf{p})\right],$$



Fermion and anti-Fermion distribution functions: $f_i(\mathbf{p}) = 1/(1+e^{[E_i^*(\mathbf{p})-\mu_i^*]/T}),$ $\bar{f}_i(\mathbf{p}) = 1/(1+e^{[E_i^*(\mathbf{p})+\mu_i^*]/T}),$

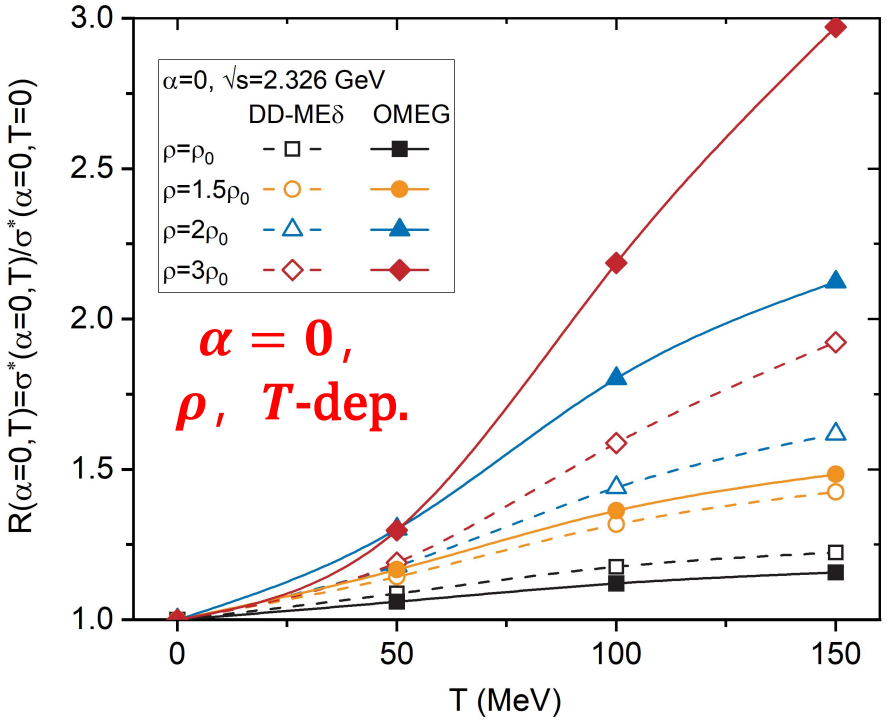


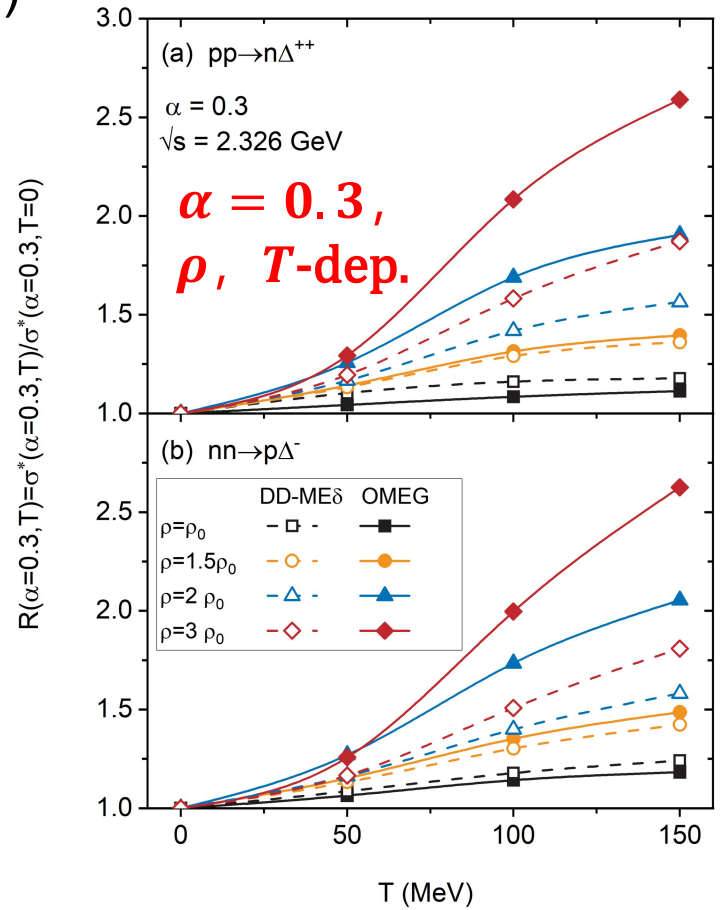


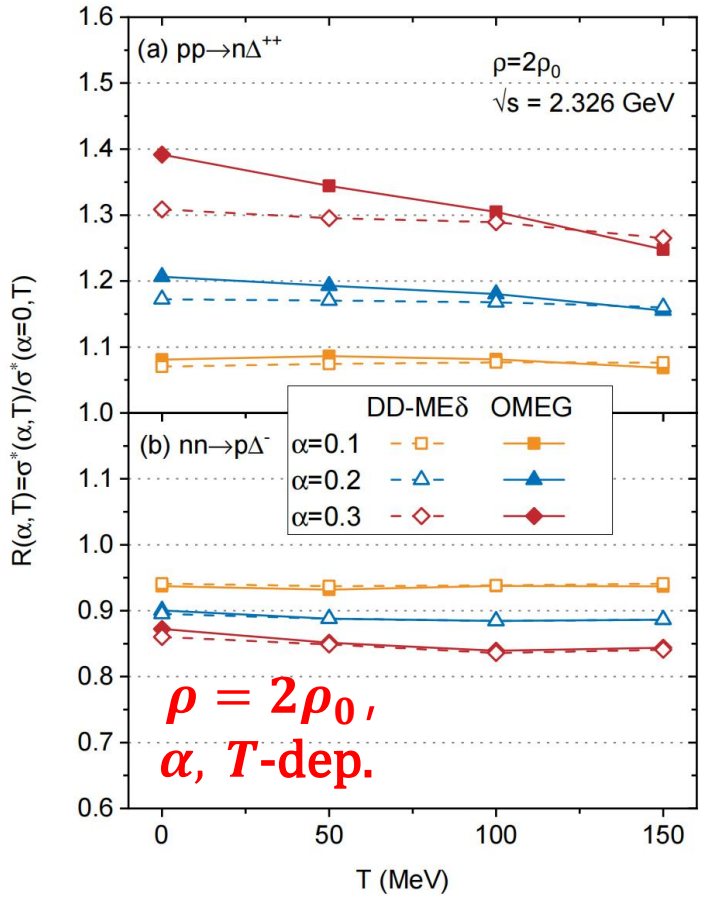
- Both coupling parameter sets yield similar temperature-dependent baryon effective mass and the mass splitting.
- The OMEG set exhibits a stronger density dependence, especially at high densities ($\rho \gtrsim 1.5\rho_0$).

Back up：NN inelastic cross section

- Temperature dependence (σ, ω, ρ, δ)







- As the temperature T increases, the Δ stiff production cross sections increase significantly.
- The ratio $R(\alpha, T)$ for both parameter sets shows similar T dependences in lower density ($\rho \leq 1.5\rho_0$), while at higher density, the model dependence becomes more obvious.
- The finite-temperature enhancement is more pronounced in isospin-symmetric matter.
- The temperature effect on the isospin dependence of the cross section is complex due to the model dependence.

Back up：NN inelastic cross section

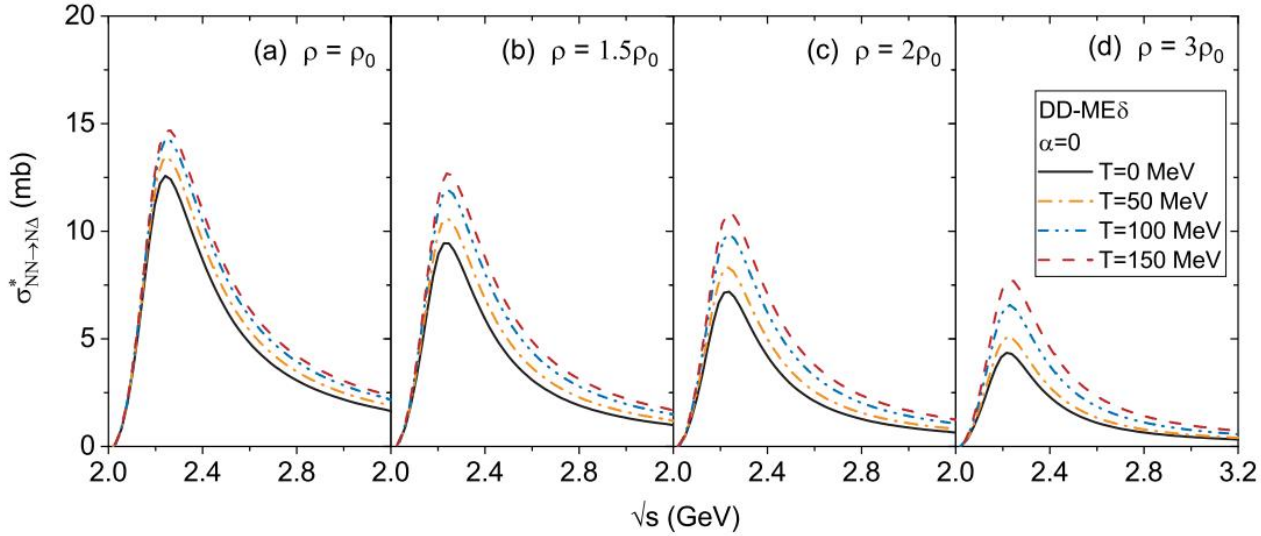


FIG. 4. (Color online) The energy, density, and temperature dependence of the $\sigma^*_{NN\to N\Delta}$ in the isospin-symmetric nuclear matter calculated with the DD-MEδ parameter set.

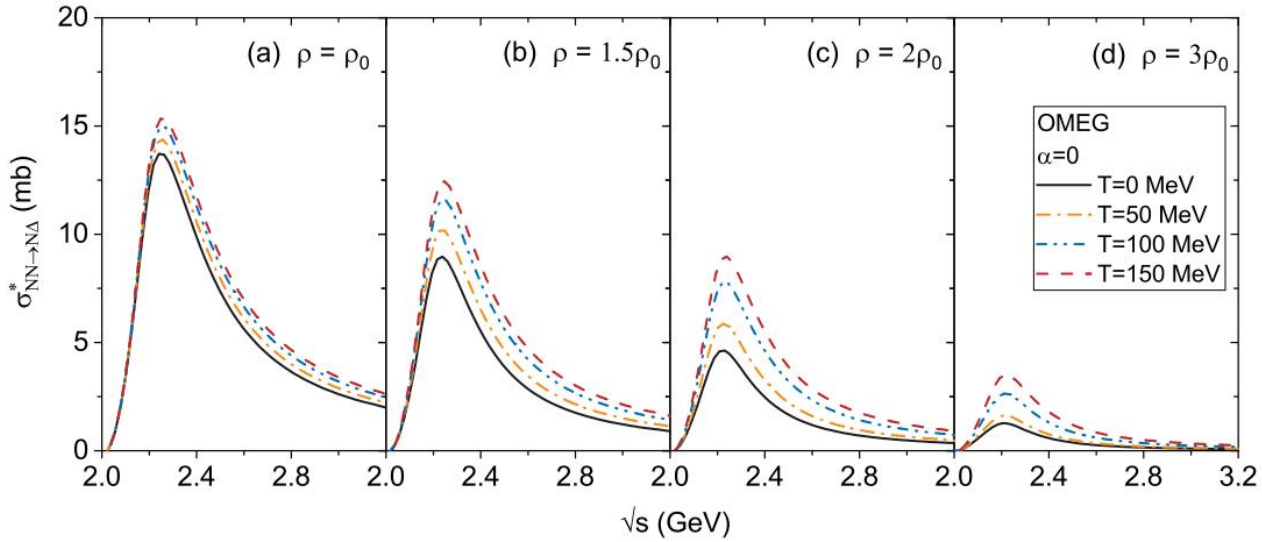


FIG. 5. (Color online) Same as Fig. 4, but for the results calculated with OMEG parameter set.

Embedding a high-momentum tail in the initial nucleus

- For nucleon *i*, the local Fermi momentum is calculated from the local density: $k_{\mathrm{F},i} = \hbar c \left[3\pi^2 \rho_i(\boldsymbol{r}_i)\right]^{1/3}.$

  The local upper boundary of the high-momentum tail (HMT) is $k_{\max,i} = \lambda k_{\mathrm{F},i}, \qquad \lambda = 2.2.$

- For a nucleus containing A nucleons, the prescribed HMT fraction is

$$f_{\mathrm{HMT}} = 0.20 \quad N_{\mathrm{pair}} = \mathrm{NINT}\left(\frac{f_{\mathrm{HMT}} A}{2}\right), \qquad N_{\mathrm{HMT}} = 2N_{\mathrm{pair}}$$

- For a non-HMT nucleon, the momentum magnitude is sampled uniformly inside its local Fermi sphere ...

- The three-dimensional HMT occupation is assumed to satisfy $n_{\mathrm{HMT}}(p) \propto \frac{1}{p^4}, \qquad k_{\mathrm{F}} < p < k_{\max}$

  the radial probability density $g_{\mathrm{HMT}}(p) = \dfrac{p^{-2}}{\dfrac{1}{k_{\mathrm{F}}} - \dfrac{1}{k_{\max}}}, \qquad k_{\mathrm{F}} < p < k_{\max}. \qquad d^3p = 4\pi p^2\, dp,$

  The cumulative probability is

$$u = \frac{\dfrac{1}{k_{\mathrm{F}}} - \dfrac{1}{p}}{\dfrac{1}{k_{\mathrm{F}}} - \dfrac{1}{k_{\max}}}, \qquad u \in [0, 1)$$

  which gives the inverse-transform sampler: $p = \left[\dfrac{1}{k_{\mathrm{F}}} - u\left(\dfrac{1}{k_{\mathrm{F}}} - \dfrac{1}{k_{\max}}\right)\right]^{-1} \quad p_i = \left[\dfrac{1}{k_{\mathrm{F},i}} - u\left(\dfrac{1}{k_{\mathrm{F},i}} - \dfrac{1}{\lambda k_{\mathrm{F},i}}\right)\right]^{-1}$

Embedding a high-momentum tail in the initial nucleus

For a common value of kF, a normalized one-body probability density per unit momentum volume may be written as

$$F(\boldsymbol{p}) = \begin{cases} (1 - f_{\mathrm{HMT}}) \dfrac{3}{4\pi k_{\mathrm{F}}^3}, & 0 \le p \le k_{\mathrm{F}}, \\ \dfrac{f_{\mathrm{HMT}}}{4\pi \left(\frac{1}{k_{\mathrm{F}}} - \frac{1}{k_{\max}} \right)} \dfrac{1}{p^4}, & k_{\mathrm{F}} < p < k_{\max}, \\ 0, & p \ge k_{\max}. \end{cases} \qquad \int F(\boldsymbol{p})\, d^3p = 1.$$

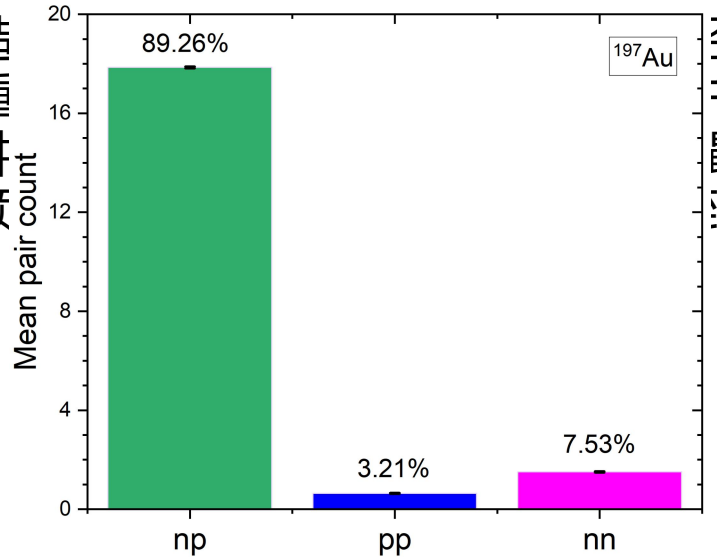
- SRC Pair-Type Selection

$$w_{np} = \xi N_p^{\mathrm{av}} N_n^{\mathrm{av}}, \quad \xi = 9$$

$$w_{pp} = \frac{N_p^{\mathrm{av}} \left(N_p^{\mathrm{av}} - 1 \right)}{2},$$

$$w_{nn} = \frac{N_n^{\mathrm{av}} \left(N_n^{\mathrm{av}} - 1 \right)}{2},$$

每成功构造
用。随后重
新计算三种
比例不是预



径使
计重
最终
到的。

- Spatial Assignment of Pair Partners $j_{\mathrm{partner}} = \arg\min_{j \in \mathcal{A}_\alpha} |\boldsymbol{r}_i - \boldsymbol{r}_j|^2$

- SRC Pair center-of-mass momenta

$$\boldsymbol{P}_{\mathrm{CM}} = \boldsymbol{p}_1 + \boldsymbol{p}_2, \qquad \boldsymbol{k}_{\mathrm{rel}} = \frac{\boldsymbol{p}_1 - \boldsymbol{p}_2}{2}.$$

$$\boxed{\boldsymbol{p}_1 = \frac{\boldsymbol{P}_{\mathrm{CM}}}{2} + \boldsymbol{k}_{\mathrm{rel}}}, \qquad \boxed{\boldsymbol{p}_2 = \frac{\boldsymbol{P}_{\mathrm{CM}}}{2} - \boldsymbol{k}_{\mathrm{rel}}}.$$

这里采用近似背对背

Each Cartesian component of the pair center-of-mass momentum is sampled independently:

$$P_{\mathrm{CM},\mu} \sim \mathcal{N}(0, \sigma_{\mathrm{CM}}^2), \qquad \mu \in \{x, y, z\}, \qquad \sigma_{\mathrm{CM}} = 0.15\ \mathrm{GeV}/c.$$

Embedding a high-momentum tail in the initial nucleus

Each Cartesian component of the pair center-of-mass momentum is sampled independently:

$$P_{\mathrm{CM},\mu} \sim \mathcal{N}(0, \sigma^2_{\mathrm{CM}}), \qquad \mu \in \{x, y, z\}, \qquad \sigma_{\mathrm{CM}} = 0.15\ \mathrm{GeV}/c.$$

The sampled vector must satisfy the spherical cutoff

$$|\boldsymbol{P}_{\mathrm{CM}}| = \sqrt{P^2_{\mathrm{CM},x} + P^2_{\mathrm{CM},y} + P^2_{\mathrm{CM},z}} \le P^{\max}_{\mathrm{CM}}, \quad P^{\max}_{\mathrm{CM}} = 0.30\ \mathrm{GeV}/c.$$

- Relative-momentum proposal and acceptance

$$k^{\mathrm{pair}}_{\mathrm{F}} = \frac{k_{\mathrm{F},1} + k_{\mathrm{F},2}}{2}, \qquad k^{\mathrm{pair}}_{\max} = \lambda k^{\mathrm{pair}}_{\mathrm{F}} \qquad k^{\mathrm{pair}}_{\mathrm{F}} < |\boldsymbol{k}_{\mathrm{rel}}| < \lambda k^{\mathrm{pair}}_{\mathrm{F}}. \qquad \boxed{k_{\mathrm{F},i} < |\boldsymbol{p}_i| < \lambda k_{\mathrm{F},i}, \qquad i = 1, 2}.$$

If either condition fails, both $\boldsymbol{k}_{\mathrm{rel}}$ and $\boldsymbol{P}_{\mathrm{CM}}$ are resampled. The current maximum number of trials is 200.

If no pair is accepted after 200 trials, the implementation sets $\boldsymbol{P}_{\mathrm{CM}}$=0, and defines the overlap of the two local HMT intervals:

$$k_{\mathrm{low}} = \max(k_{\mathrm{F},1}, k_{\mathrm{F},2}),$$
$$k_{\mathrm{high}} = \min(\lambda k_{\mathrm{F},1}, \lambda k_{\mathrm{F},2}).$$
$$k_{\mathrm{low}} < |\boldsymbol{k}_{\mathrm{rel}}| < k_{\mathrm{high}}, \qquad \boldsymbol{p}_1 = \boldsymbol{k}_{\mathrm{rel}}, \qquad \boldsymbol{p}_2 = -\boldsymbol{k}_{\mathrm{rel}}. \qquad \boldsymbol{p}_1 + \boldsymbol{p}_2 = \boldsymbol{0}.$$

- Residual Center-of-Mass Correction

After assigning all momenta, the residual nuclear momentum is $\boldsymbol{P}_{\mathrm{res}} = \sum_{i=1}^{A} \boldsymbol{p}_i.$

The residual is redistributed over the non-HMT background $\boldsymbol{p}'_j = \boldsymbol{p}_j - \frac{\boldsymbol{P}_{\mathrm{res}}}{N_{\text{non-HMT}}}, \qquad j \in \text{non-HMT}.$

If the corrected momentum exceeds its local Fermi momentum, it is rescaled: $\boldsymbol{p}'_j \longrightarrow \boldsymbol{p}'_j \frac{k_{\mathrm{F},j}}{|\boldsymbol{p}'_j|}.$

Because this rescaling can generate another small residual momentum, the correction is iterated 20 times. The numerical target is therefore $\left| \sum_{i=1}^{A} \boldsymbol{p}_i \right| \approx 0.$